Effect of precursor mineralogy on the thermal infrared emission spectra of hematite: Application to Martian hematite mineralization

T. D. Glotch
Department of Geological Sciences, Arizona State University, Tempe, Arizona, USA

R. V. Morris
NASA Johnson Space Center, Houston, Texas, USA

P. R. Christensen and T. G. Sharp
Department of Geological Sciences, Arizona State University, Tempe, Arizona, USA

Received 7 December 2003; revised 10 April 2004; accepted 10 May 2004; published 13 July 2004.

[1] Observations from the Thermal Emission Spectrometer (TES) instrument aboard the Mars Global Surveyor (MGS) spacecraft led to the discovery of two isolated deposits of gray, crystalline hematite located in Meridiani Planum and Aram Chaos and several smaller deposits in Valles Marineris. Several pathways for formation of these hematite deposits have been proposed, involving both aqueous and nonaqueous processes. This work uses the precise shape and position of spectral features in the Martian hematite thermal emission spectrum to constrain hematite formation pathways. Thermal infrared emission spectra, X-ray powder diffraction patterns, Mössbauer spectra, and transmission electron microscope (TEM) photomicrographs were obtained for synthetic and natural hematite samples derived by (1) dehydroxylation of fine-grained goethite and (2) oxidation of magnetite. Collectively, the instrumental analyses show that the mineralogical composition and crystal morphology of precursor samples and the time and temperature conditions under which decomposition to hematite occur determine the crystallinity and crystal morphology of the hematite product. Comparison of laboratory and MGS-TES spectra shows that the Martian hematite spectra correspond closely with a synthetic hematite sample derived by pseudomorphic and topotactic dehydroxylation of goethite at 300°C. Spectra of goethite-precursor samples dehydroxylated at higher temperatures provide increasingly poor fits. Spectra of hematite samples derived by high-temperature thermal oxidation of magnetite are also poorer fits to the Martian hematite spectrum. Thermal emission spectra of goethites heated at lower temperatures are characterized by the spectral signatures of both hematite and goethite and are not consistent with the Martian spectra. The characteristic that distinguishes the synthetic hematite sample with the Mars-like spectral signature from the other synthetic hematite samples is the high proportion of crystal surfaces that are crystallographic {001} faces (**c** faces) for the former but not the latter. The high proportion of {001} face area results because the largest surface of the lath-shaped hematite particles is the (001) face, as determined by TEM. Thus a possible formation pathway for hematite in Meridiani Planum, Aram Chaos, and Valles Marineris is precipitation of goethite from aqueous solutions as lath-shaped crystals, possibly as a stain, cement, and/or massive deposit, followed by pseudomorphic and topotactic dehydroxylation to hematite at temperatures below ~300°C. *INDEX TERMS:* 6225 Planetology: Solar System Objects: Mars; 3672 Mineralogy and Petrology: Planetary mineralogy and petrology (5410); 1060 Geochemistry: Planetary geochemistry (5405, 5410, 5704, 5709, 6005, 6008); *KEYWORDS:* hematite, Mars, TES

Citation: Glotch, T. D., R. V. Morris, P. R. Christensen, and T. G. Sharp (2004), Effect of precursor mineralogy on the thermal infrared emission spectra of hematite: Application to Martian hematite mineralization, *J. Geophys. Res.*, *109*, E07003, doi:10.1029/2003JE002224.

0148-0227/04/2003JE002224$09.00

1. Introduction

[2] Isolated deposits of gray, crystalline hematite have been identified on the Martian surface at Meridiani Planum, Aram Chaos, Candor Chasma, and Ophir Chasma using data returned from the Thermal Emission Spectrometer (TES) instrument aboard the Mars Global Surveyor (MGS) spacecraft [*Christensen et al.*, 2000, 2001a]. *Christensen et al.* [2000] listed five hypotheses regarding the formation of crystalline hematite on Mars: (1) low-temperature precipitation of Fe oxides/hydroxides from standing, oxygenated, Fe-rich water, followed by subsequent alteration to gray hematite, (2) low-temperature leaching of iron-bearing silicates and other materials leaving a Fe-rich residue (laterite-style weathering) which is subsequently altered to gray hematite, (3) direct precipitation of gray hematite from Fe-rich circulating fluids of hydrothermal or other origin, (4) formation of gray hematite surface coatings during weathering, and (5) thermal oxidation of magnetite-rich lavas.

[3] Since this initial work, several authors have examined the geomorphology and/or spectral character of the deposits to determine hematite formation mechanisms. *Lane et al.* [2002] cited the absence of a 390 cm^{-1} absorption in the Martian hematite spectrum as evidence for platy hematite grains, where the area of the (001) face (**c** face) is large compared to other faces. Their model for the formation of the deposits includes deposition of any combination of iron oxides or oxyhydroxides by aqueous or hydrothermal fluids, burial, and metamorphism to gray platy hematite grains, followed by exhumation in recent times. On the basis of a detailed geomorphic examination of the Sinus Meridiani region, *Hynek et al.* [2002] conclude that the most likely method of hematite formation was either emplacement by a hydrothermal fluid or oxidation of a magnetite-rich pyroclastic deposit. Similarly, *Arvidson et al.* [2003] and *Chapman and Tanaka* [2002] favor a model involving the alteration of pyroclastic deposits by aqueous or hydrothermal fluids. *Calvin et al.* [2003] and *Fallacaro and Calvin* [2003] prefer a model of deposition analogous to terrestrial banded iron formation (BIF) deposits. On the basis of geochemical modeling and an examination of Aram Chaos, *Catling and Moore* [2003] favor emplacement by hydrothermal fluids with a minimum temperature of 100°C. *Kirkland et al.* [2004] argue that the deposits in Meridiani Planum are composed of "fine intimate" hematite, possibly in the form of coatings. All of these models are derivatives of the original five formation processes suggested by *Christensen et al.* [2000]. Finally, it has also been suggested that phosphorus may have played an important role in the formation of Martian hematite [*Barron et al.*, 2004; *Greenwood et al.*, 2004].

[4] To provide constraints for hematite formation pathways on Mars, we measured thermal emission spectra for a series of synthetic and natural hematite samples with different precursor mineralogy and particle morphology, formation temperature, and crystallinity. We also obtained powder X-ray diffraction and Mössbauer data for synthetic and natural hematites, and we characterize particle shape and size and degree of post-transformation crystal growth by transmission electron microscopy (TEM). We conclude with a comparison of laboratory and MGS-TES hematite spectra and the implications thereof for hematite formation pathways on Mars.

2. Background

[5] The MGS-TES instrument is a Fourier-Transform Michelson Interferometer (FTIR) that covers the wave number range from ~1700 to 200 cm^{-1} (~6 to 50 μm) at 5 or 10 cm^{-1} spectral sampling. Each detector has an instantaneous field of view of ~8.5 mrad, providing a spatial resolution of ~3 by 3 km. From the final TES mapping orbit of ~380 km, the actual surface sampling is 3 × ~8 km. The elongated pixel dimension results from the final mapping orbit of MGS, which is opposite in direction of that originally planned, and the fact that the planned image motion compensation could not be used. It also has two broadband radiometers which measure energy in the thermal (~5–100 μm) and visible/near-infrared (~0.3–3.5 μm) wavelengths. The focal planes in each wavelength interval consist of 6 detectors arranged in a 3 by 2 array. For a complete description of the TES instrument and instrument operations, see *Christensen et al.* [2001b].

[6] Comparison of the average Martian hematite spectrum measured by MGS-TES to hematite emissivity spectra for a variety of naturally occurring hematites shows small but important differences [*Lane et al.*, 2002]. In particular, band shapes, positions, and relative intensities of hematite spectra vary over the range of samples. These differences imply that the IR spectral effects caused by the natural variability of hematite have not been fully characterized, especially with respect to the formation pathway and crystal morphology.

[7] Using the target transformation and factor analysis method of *Bandfield et al.* [2000, 2002], we recovered a hematite spectrum from ocks 1583 through 7000 of the MGS-TES data (ock 1 is equivalent to MGS mapping orbit 1683; some science phasing orbit data were used in this study) for two areas in Meridiani Planum (5°S to 0°, 356.0° to 356.2°E and 3°S to 2°N, 358.6° to 358.8°E) and one in Aram Chaos (3° to 4°N, 339° to 340°E). Because the hematite component varies independently of the basalt in the three scenes, we were able to recover spectra that are representative of just the hematite. The resulting three hematite spectra are nearly identical and were averaged to produce a single Martian hematite spectrum. Figure 1 shows the three recovered hematite spectra and the average hematite spectrum. The average Martian hematite spectrum has major emissivity minima centered at 539, 445, and 303 cm^{-1}. The broad atmospheric CO_2 fundamental absorption centered at 667 cm^{-1} prevented the use of additional spectral channels at higher wave numbers.

3. Samples and Methods

3.1. Sample Preparation

[8] Three types of hematite samples were studied: (1) hematite synthesized by thermal decomposition of three different synthetic goethite precursors, (2) hematite synthesized by thermal oxidation of two different synthetic magnetite precursors, and (3) three naturally occurring hematite samples from various geologic provinces. Table 1

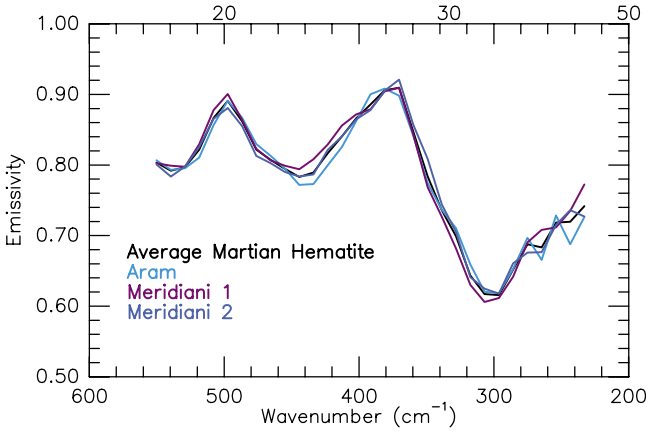

Figure 1. Target transformation derived hematite spectra from Meridiani Planum and Aram Chaos. The nearly identical spectra imply a common formation mechanism. No contrast enhancement was performed on the spectra.

shows the names, precursor mineral, precursor crystal size, and formation temperature for the synthetic goethite and magnetite precursor samples that were altered to hematite. The nomenclature shows whether a sample has been heated or not and at what temperature the heating occurred (e.g., GTS2 versus GTSH2-300).

[9] The synthetic hematite samples were pressed at 10,000 psi in a hydraulic hand press into compact pellets to increase the contrast of their IR spectra [*Salisbury and Wald*, 1992; *Johnson et al.*, 1998]. In all cases, samples were compacted after heating to minimize particle sintering. Spectra of samples pressed at higher and lower pressures did not deviate significantly from those pressed at 10,000 psi.

3.1.1. Goethite-Precursor Series

[10] Goethite precursors used in this study are synthetic yellow-orange powders obtained from Pfizer, Inc. Samples GTS2 and GTS3 are described by *Morris and Lauer* [1981] and *Morris et al.* [1985], and they have mean crystal dimensions of 0.05 × 0.4 μm and 0.1 × 0.7 μm, respectively. According to the manufacturer, GTS4 was synthesized by the same direct precipitation method as GTS2 and GTS3 and has a mean crystal dimension (as supplied by the manufacturer) of ∼1.5 μm in the long direction. Each material was heated in air in an Omegalux LMF 3550 furnace at temperatures of 250°, 300°, 400°, 500°, 600°, and 700°C for 24 hours and then cooled slowly over a period of 2 to 3 hours. According to *Morris and Lauer* [1981], dehydroxylation of GTS2 and GTS3 is complete by 280°C at a heating rate of ∼0.5°C/min from ambient temperature. Each final product of heating is a red powder.

3.1.2. Magnetite-Precursor Series

[11] Magnetite precursors used in this study are the black powder samples MTS4 and MTS5 described by *Morris et al.* [1985]. MTS4 was synthesized by direct precipitation from solution, and MTS5 was prepared by dehydroxylation of acicular goethite to hematite and subsequent reduction of the hematite to magnetite. Mössbauer spectra of both powders show that these samples are cation-deficient relative to stoichiometric magnetite [*Morris et al.*, 1985]. The mean crystal dimensions of these samples are 0.5 μm for the equant MTS4 crystals and 0.09 × 0.6 μm for the acicular MTS5 crystals. Samples of each material were oxidized by heating in air for 24 hours in a furnace at temperatures of 300°, 400°, 500°, 600°, and 700°C and then allowed to cool slowly over 2 to 3 hours. Like the goethite-precursor series, each final product of heating is a red powder.

3.1.3. Natural Hematite Samples

[12] Three natural gray hematite samples were selected on the basis of variability of geologic setting and inferred formational mechanisms.

[13] Hematite-bearing sample SWAN1 is a quartz-rich fault breccia coated with black-gray hematite collected near Swansea, Arizona. The rock is heavily weathered throughout (red colored) with only the surface layer gray-black. The hematite was likely deposited as a vein in the quartz country rock (J. Michalski, personal communication, 2003).

[14] The hematite deposits in the Swansea mine district and the surrounding Buckskin and Rawhide Mountains are the result of mineralization related to Miocene extensional tectonism. Hematite mineralization was one of several related processes that included K metasomatism of sedimentary and volcanic rocks, chloritic alteration of brecciated rocks below the regional detachment faults, Cu-Fe mineralization along the detachment faults, hydrothermal carbonate replacement of rocks above the detachment faults, and sedimentary and fracture-filling Mn mineralization [*Spencer and Welty*, 1989]. Studies of fluid inclusions in rocks near Swansea indicate that the

Table 1. Summary of Precursor History and Formation Temperature of Synthetic Samples

Sample	Formation Temperature, °C	Precursor History	Precursor Grain Size, μm
GTSH2-250	250	goethite	0.05 × 0.4
GTSH2-300	300	goethite	0.05 × 0.4
GTSH2-400	400	goethite	0.05 × 0.4
GTSH2-500	500	goethite	0.05 × 0.4
GTSH2-600	600	goethite	0.05 × 0.4
GTSH2-700	700	goethite	0.05 × 0.4
GTSH3-250	250	goethite	0.1 × 0.7
GTSH3-300	300	goethite	0.1 × 0.7
GTSH3-400	400	goethite	0.1 × 0.7
GTSH3-500	500	goethite	0.1 × 0.7
GTSH3-600	600	goethite	0.1 × 0.7
GTSH3-700	700	goethite	0.1 × 0.7
GTSH4-250	250	goethite	∼1.5 (long direction)
GTSH4-300	300	goethite	∼1.5 (long direction)
GTSH4-400	400	goethite	∼1.5 (long direction)
GTSH4-500	500	goethite	∼1.5 (long direction)
GTSH4-600	600	goethite	∼1.5 (long direction)
GTSH4-700	700	goethite	∼1.5 (long direction)
MTSH4-300	300	magnetite	0.5
MTSH4-400	400	magnetite	0.5
MTSH4-500	500	magnetite	0.5
MTSH4-600	600	magnetite	0.5
MTSH4-700	700	magnetite	0.5
MTSH5-300	300	goethite → magnetite	0.09 × 0.6
MTSH5-400	400	goethite → magnetite	0.09 × 0.6
MTSH5-500	500	goethite → magnetite	0.09 × 0.6
MTSH5-600	600	goethite → magnetite	0.09 × 0.6
MTSH5-700	700	goethite → magnetite	0.09 × 0.6

hydrothermal fluids were saline (12–24 wt.% NaCl equiv.) and had temperatures between 175°C and 300°C [*Wilkins et al.*, 1986; *Roddy et al.*, 1988].

[15] Two massive gray hematite samples (provided by S. Reynolds) were studied. Sample DUR1 is from the Cerro de Mercado iron deposits, part of the Mercado Iron Member of the Cacaria Formation near Durango, Mexico. The coarse-grained hematite in these deposits was derived by the oxidation of magnetite [*Lyons*, 1988]. The original iron deposits were emplaced during a break in the two major eruptive cycles of the 30 Ma Chupaderos caldera. The iron deposit was the result of an eruption of an iron-rich magma that also had large amounts of fluorine, chlorine, carbon dioxide, and water. Iron oxides were originally magnetite, but in the late stages of volcanic activity, large volumes of halogen-rich gases flowed through the iron deposits and oxidized the magnetite to hematite [*Lyons*, 1988].

[16] The other massive gray hematite sample (ODH3) is from the Olympic Dam ore in southern Australia [*Oreskes and Einaudi*, 1992; *Haynes et al.*, 1995]. The Olympic Dam deposit is located in the mid-Proterozoic granite basement of South Australia and contains over 2 billion tons of Cu-U-Au-Ag-(REE) mineralization [*Scott*, 1987]. The deposits are composed of steeply dipping breccia columns and dikes formed by mechanical brecciation and hydrothermal metasomatism of the host granite. In rare cases, hematite is formed as an oxidation product of magnetite, but the widespread hematite replacement of the host granite implies direct precipitation from hydrothermal fluids. Hematite occurs additionally as coarse-grained (1–10 mm), black, euhedral crystals in massive bodies, fragments, and vugs in the hematite-rich breccias and as fine-grained hematite laths (5–50 μm) intergrown with barite and sericite [*Oreskes and Einaudi*, 1992]. Stable oxygen isotopes indicate that hematite was emplaced by fluids ($\delta^{18}O < 9‰$) at temperatures of 200°–400°C [*Oreskes and Einaudi*, 1992]. The sample examined in this study is the massive, hydrothermally emplaced variety.

3.2. Laboratory Sample Analysis

[17] Thermal infrared (200–2000 cm^{-1}) emission spectra were collected at 2 cm^{-1} sampling (4 cm^{-1} spectral resolution) on Arizona State University's modified Nicolet Nexus 670 E.S.P. Fourier-Transform Infrared (FTIR) spectrometer. Each pressed-pellet sample spectrum is an average of 270 scans collected while the samples were maintained at 80°C. The natural hematites studied here are in the form of hand samples, and only 180 scans were collected. The rock samples were not actively heated, and fewer scans were collected in order to facilitate rapid spectral measurement and prevent the introduction of a slope resulting from sample cooling. Details of the collection procedure, laboratory setup, and calibration process are given by *Christensen and Harrison* [1993] and *Ruff et al.* [1997]. Visible-Near IR measurements were made on a Cary-14 Diffuse Reflectance Spectrometer. For details on the instrument and procedure, see *Morris et al.* [2000].

[18] TEM images were acquired on ASU's Phillips CM200 FEG microscope run at a 200 kV potential. It is equipped with a field emission gun and a side entrance stage and has a supertwin objective lens for imaging and diffraction. Samples were prepared by dispersing a powdered sample in acetone and covering a holey-carbon-film-covered grid with the dispersed sample.

[19] Powder X-ray diffraction spectra were collected on Johnson Space Center's Scintag XDS2000 with a Cu-Kα source. X-ray patterns were collected over a range of 2θ angles from 2–70 degrees.

[20] Transmission Mössbauer spectra were acquired at room temperature on Johnson Space Center's Ranger Scientific spectrometers [*Morris et al.*, 1985, 1989] with a ^{57}Co(Rh) source at an intensity of ~25 mCi. Velocity calibration was done with a laser interferometer. Absorbers were made by dispersing powdered samples in epoxy to a density of 50–100 kg/m^2 of Fe. Mössbauer parameters were derived by an in-house computer program (JSCFIT) using theoretical line shapes to fit folded spectra. Derived parameters are the isomer shift (IS) relative to the midpoint of the spectrum of metallic iron foil at 293 K, quadrupole shift (QS), hyperfine field strength (B_{hf}), and full widths at half maximum intensity (FWHM). Typical uncertainties are ±0.01 mm/s for IS and QS, ±0.2 T for B_{hf}, and ±0.02 mm/s for FWHM [*Morris et al.*, 2000].

4. Results

4.1. Visible and Near-IR (VNIR) Measurements

[21] Vis-Near IR spectra were acquired for the three natural gray hematite samples (Figure 2). All of the natural surfaces exhibit a weak red hematite spectral signature. In contrast, the surface of SWAN1 obtained by sawing and polishing with 60 grit paper has a strong red hematite spectral signature. The pressed synthetic samples are purple-red to the eye and presumably would also have spectral signatures characteristic of red hematite.

4.2. TEM

[22] In general, our TEM observations of air-heated fine powders of goethite and magnetite parallel the results of previous studies summarized by *Cornell and Schwertmann* [1996]. We summarize our observations below.

4.2.1. GTSH Series

[23] TEM photomicrographs and selected-area electron diffraction patterns were acquired for several synthetic hematite samples that were chosen to represent the broad range of precursor minerals and formation temperatures used in this study. Images of samples GTSH2-300 (Figure 3) and GTSH3-300 show hematite crystals that are pseudomorphic after goethite. Inspection shows that these hematite crystals are the same size and shape as the precursor goethite crystals. Indexing of the diffraction pattern indicates pure hematite with the [001] axis perpendicular to the plane of the bladed (lath-shaped) crystals.

[24] In contrast to the low-temperature GTSH samples, the high-temperature samples show evidence of recrystallization and sintering (Figures 4a and 4b). Very little evidence of original goethite morphology is present. Individual hematite crystals appear to be rod shaped and are much smaller (<0.5 μm) than the goethite precursor crystals.

4.2.2. MTSH Series

[25] Photomicrographs of sample MTSH4-700 (Figure 5a) show small equant euhedral to anhedral crystals. There is

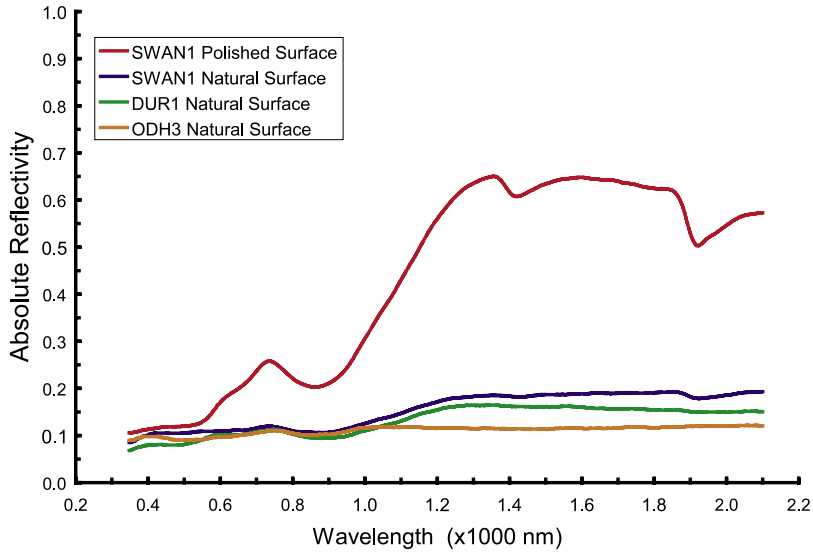

Figure 2. Vis-Near IR spectra of the natural hematite samples. All samples display some red hematite-like features. Only the polished slab of sample SWAN1 has a strong red hematite spectrum.

little evidence for the precursor octahedral morphology (Figure 5b) of the magnetite precursor, and extensive sintering of the crystals has taken place.

[26] Photomicrographs acquired of sample MTSH5-500 show flat, blade-shaped crystals that have been slightly modified by recrystallization and sintering (Figure 6a). This is consistent with the fact that the MTS5 precursor was goethite that was oxidized to hematite and then reduced to magnetite. Comparison to the GTSH2-300 and GTSH3-300 samples shows that the MTSH5-500 sample crystals are more rounded and have a higher aspect ratio (0.15 versus ~0.13 for the GTSH samples). Higher magnifications (Figure 6b) show small (~10–100 nm) holes in many of the crystals that were not apparent in any of the GTSH samples.

4.3. X-Ray Diffraction

4.3.1. Synthetic Samples

[27] A subset of synthetic hematite samples were selected for powder X-ray diffraction analysis to confirm phase identifications and to follow changes in crystallinity during heating. Diffraction patterns of samples from the GTSH2 series (Figure 7a) indicate an increase in hematite crystallinity as the heating temperature of goethite increases. The increase in crystallinity is marked by the narrowing of width and increase in intensity of the peak at $2\theta = 33.5°$. The selected line broadening of the low-temperature hematites results from the incomplete ordering of cations in the hematite crystal structure. The cation arrangement becomes highly disordered as goethite transforms to hematite at temperatures below 600°C. The oxygen framework, however, undergoes only a slight structural rearrangement as goethite is transformed into hematite, leading to the observed sharp lines. Heating goethite at temperatures above 600°C allows the cations to rearrange, and the XRD peaks sharpen [*Cornell and Schwertmann*, 1996].

[28] X-ray diffraction patterns confirm the presence of maghemite in sample MTSH4-400. Maghemite peaks are present at $2\theta = 15.2°$, 26.4°, and 30.5° but are absent from the pure hematite sample MTSH4-700 (Figure 7b) [*Cornell and Schwertmann*, 1996]. The same pattern of line width narrowing is present in the hematite peaks of these samples, again showing the increase in crystallinity at higher thermal decomposition temperatures.

4.3.2. Natural Samples

[29] XRD powder patterns of samples DUR1, SWAN1, and ODH3 (Figure 7c) exhibit characteristics similar to

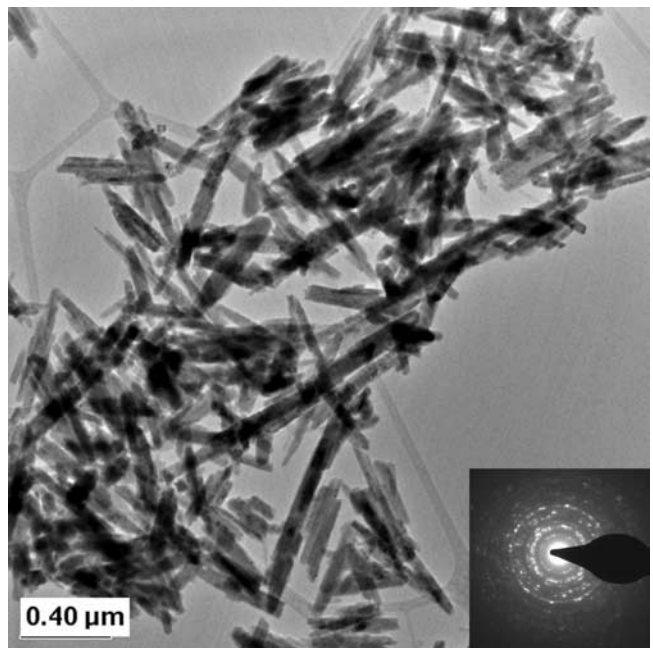

Figure 3. TEM photomicrograph of hematite sample GTSH2-300. At low hematite formation temperatures, the acicular structure of the goethite precursor is well preserved. The inset shows the diffraction pattern used to confirm mineral identification and axis orientation.

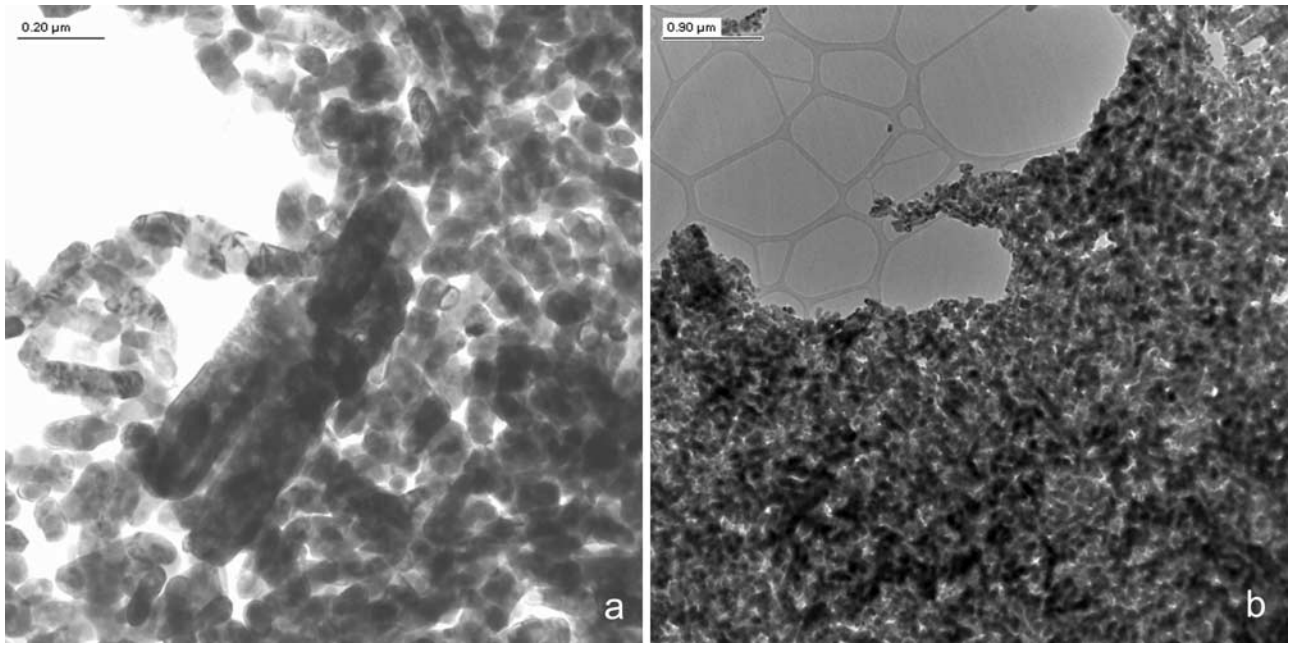

Figure 4. TEM photomicrographs of hematite sample GTSH2-700. At higher formation temperatures, the hematite recrystallizes into small (<1 μm) crystallites that are sintered together. (a) A high-magnification image of the sintered hematite crystallites. (b) At lower magnification the hematite appears as a coarse crystalline mass.

those of the synthetic hematite samples, along with peaks from additional oxide and nonoxide phases. The XRD pattern of sample DUR1 shows sharp peaks, indicating the presence of well-crystalline hematite. Sample ODH3 is composed largely of well-crystalline hematite, along with minor peaks for quartz (2θ = 21.0° and 26.8°), a phyllosilicate (2θ = 8.9°), and, tentatively, a sulfide (2θ = 46.9°).

[30] The XRD pattern of sample SWAN1 was acquired from a sample representative of the bulk rock. It is dominated by quartz, the main component of the host rock upon which the hematite rind occurs. The hematite peaks resemble

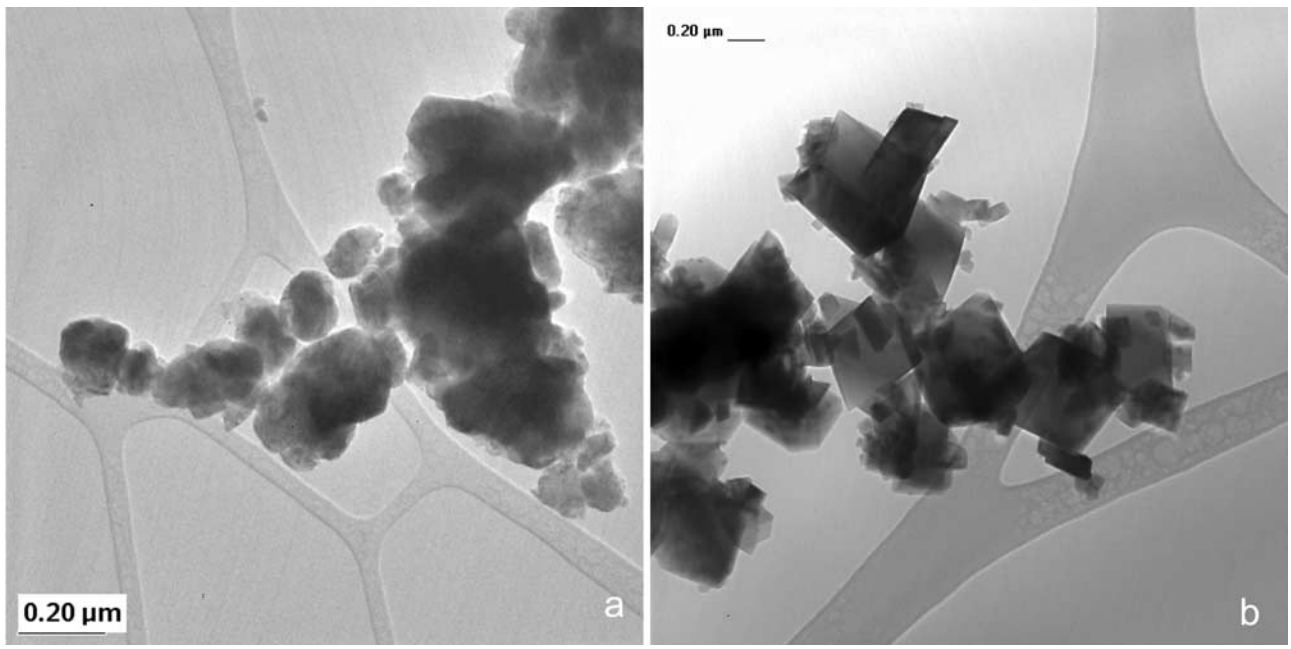

Figure 5. TEM photomicrographs of sample MTSH4-700 and precursor magnetite. (a) Hematite sample MTSH4-700. The octahedral structure of the magnetite precursor is poorly preserved, and some crystals are sintered together. (b) Magnetite sample MTS5. Note the octahedral crystal habit and the sharp edges of the crystals.

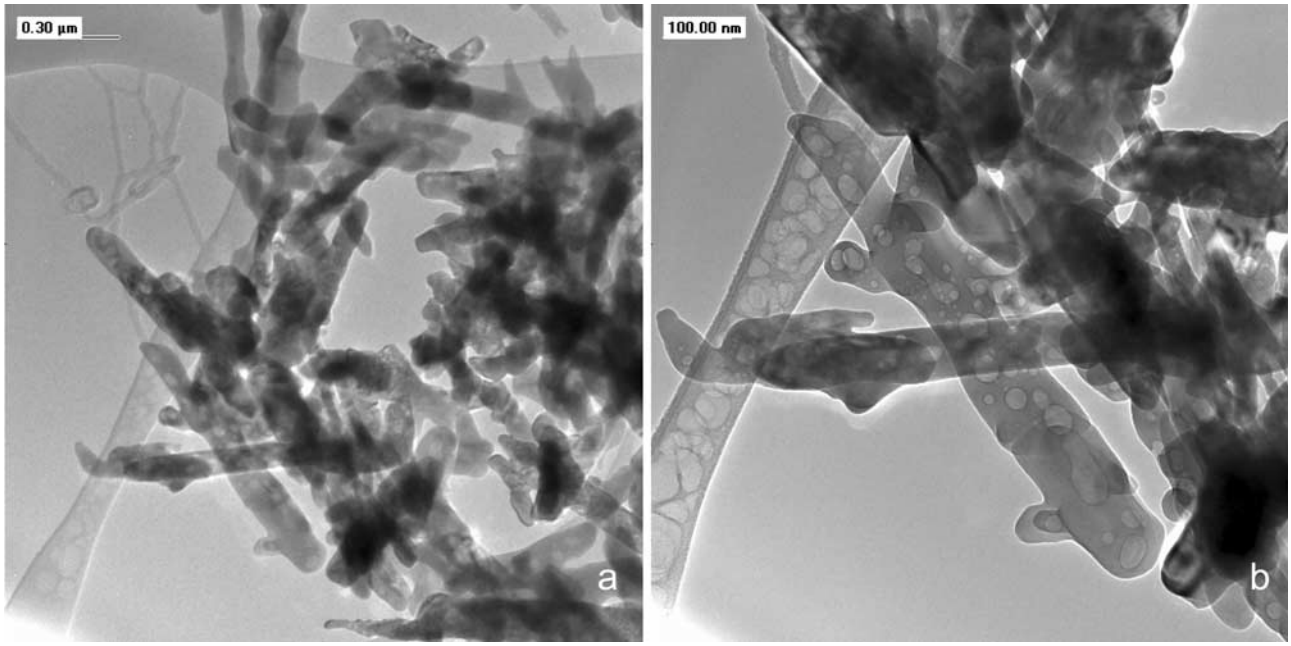

Figure 6. TEM photomicrographs of hematite sample MTSH5-500. (a) The acicular structure of the magnetite precursor (formed by reduction of goethite) is evident, but not as well preserved as hematite formed from goethite at low temperatures. (b) At high magnification the hematite laths have a spongy texture. Note that the linear structure on the far left of the image is not a hematite lath, but a carbon fiber.

those in sample GTSH2-300, with broad and narrow peaks occurring at $2\theta = 33.5°$ and 35.8°, respectively. A minor goethite component is also present, as shown by the broad peak at $2\theta = 21.7°$.

4.4. Mössbauer Spectra

4.4.1. Synthetic Samples

[31] A subset of the synthetic hematite samples were selected for Mössbauer analysis. Mössbauer spectra of the synthetic goethite and magnetite precursors and the hematite samples derived from them are shown in Figure 8a. The isomer shift (IS), quadrupole splitting (QS), magnetic hyperfine field (B_{hf}), and the full width half maximum intensity of the first and sixth lines of the sextets (FWHM) are summarized in Table 2 along with corresponding parameters for the natural hematites analyzed in this study and three synthetic hematites reported by *Morris et al.* [1985]. HMS3 was prepared by direct precipitation from solution, and HMS12 and HMS14 were synthesized, like the samples in this study, by heating goethite and magnetite precursors, respectively. Except for MTSH4-700, which has a somewhat high value of B_{hf}, the values of IS, QS, and B_{hf} are the same within error and in agreement with literature values for hematite [e.g., *Stevens et al.*, 1998]. The larger values of FWHM, particularly for samples heated at 300°–400°C, are consistent with a poorly ordered cation framework for these samples as observed in the XRD spectra. In agreement with our thermal emission and XRD results, the Mössbauer spectrum of MTSH4-400 has a second sextet whose Mössbauer parameters imply maghemite. On the basis of peak areas, the sample is ~40% maghemite. Residual precursor phases (goethite and magnetite) were not detected in any of the heated samples.

4.4.2. Natural Samples

[32] The Mössbauer spectra of the natural hematite samples examined in this study are shown in Figure 8b. In addition, IS, QS, B_{hf}, and FWHM are reported in Table 2. Sample DUR1 has values of IS, QS, B_{hf}, and FWHM consistent with well-ordered hematite. These values are similar for sample ODH3, although it is apparent from the Mössbauer spectrum that some impurities are present in the sample. Similar to the synthetic samples heated at 300°–400°C, SWAN1 has a large FWHM value, consistent with poorly ordered hematite. An additional doublet in the SWAN1 Mössbauer spectrum is consistent with minor (superparamagnetic) goethite. Like the sample used for the XRD analysis, the sample of SWAN1 used for Mössbauer analysis is representative of the bulk rock, and not just the hematite rind.

4.5. Thermal Emission Spectra

4.5.1. GTSH2 Series

[33] Previous work [*Rendon and Serna*, 1981] has shown that IR absorption spectra of goethite-derived hematite depend greatly on the temperature of transformation. Our work shows that this is also the case for thermal emission spectra. Emission spectra of the GTSH2 series are shown in Figure 9, and significant changes in spectral shape with increasing dehydroxylation temperature are observed. For this and subsequent figures the 800–1200 cm^{-1} region of the spectrum is not shown because coarse-particulate oxide minerals do not have features there [*Christensen et al.*, 2000; *Lane et al.*, 2002]. The GTS2 precursor and sample GTSH2-250 (GTS2 precursor, heated to 250°C) have similar spectra. Both the GTS2 and the GTSH2-250 spectra have emissivity minima at 893 and 795 cm^{-1}, consistent with goethite, that are not present in hematite spectra. These two bands represent O-H bending modes in the goethite crystal [*Cambier*, 1986]. As the goethite loses water in its transformation to hematite, these bands disappear. Additional emissivity

minima are present at 600, 468, 427, 406, and 268 cm^{-1} in each spectrum, although the 600 cm^{-1} minimum is very weak in the GTSH2-250 spectrum. There is no indication of hematite spectral features in either the GTS2 or GTSH2-250 spectra. The lowest heating temperature at which hematite features appear in the emissivity spectra is 300°C (sample GTSH2-300). The absorption bands at 893 and 795 cm^{-1} seen in the GTSH2 and GTSH2-250 spectra are not present in the GTSH2-300 spectrum. A strong absorption band is also present at 541 cm^{-1} in the GTSH2-300 spectrum. Additionally, the broad absorptions at 468 and 406 cm^{-1} in the GTS2 and GTSH2-250 spectra are replaced by a single emissivity minimum at 444 cm^{-1} in the GTSH2-300 spectrum. The minimum at 268 cm^{-1} seen in the GTS2 and GTSH2-250 spectra is replaced by a 305 cm^{-1} minimum, with a resultant shift of the emissivity maximum from 310 to 371 cm^{-1} in the GTSH2-300 spectrum. For samples GTSH2-500 and higher-temperature samples, an absorption at 385 cm^{-1} appears and becomes more pronounced as the temperature of dehydroxylation increases. An additional effect of the increasing heating temperature is the effective broadening of the absorption band at 541 cm^{-1}.

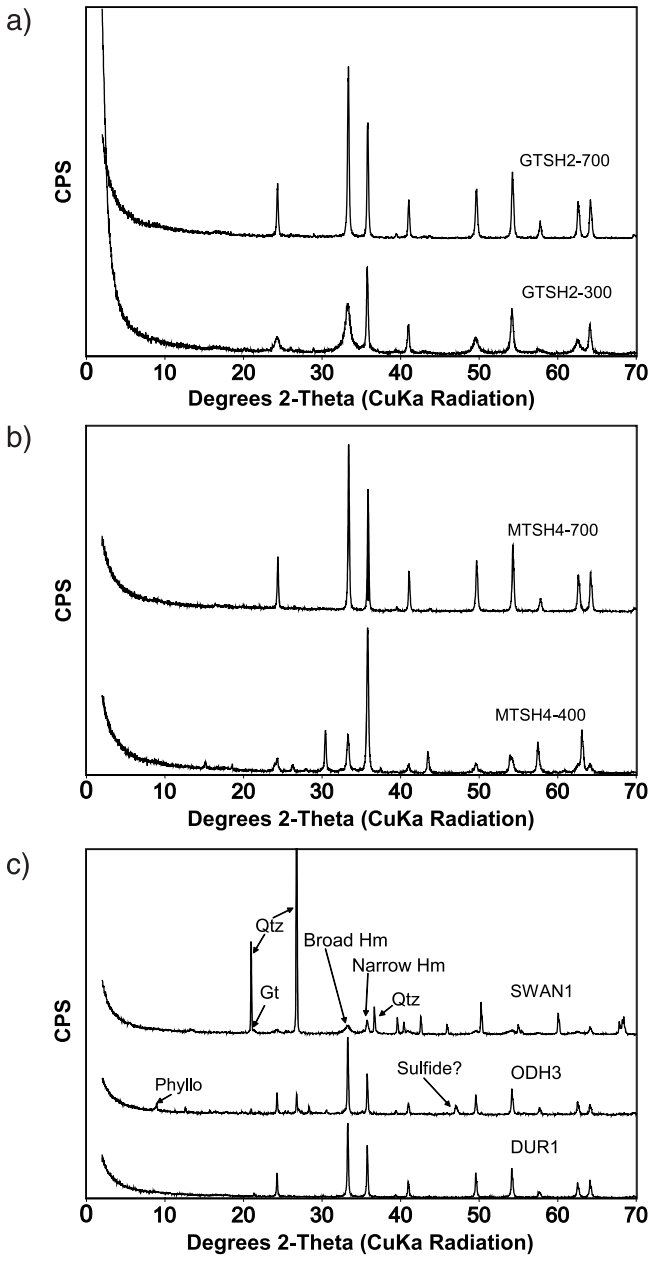

Figure 7. X-ray diffraction patterns of selected synthetic hematite samples. (a) X-ray diffraction patterns of goethite-derived samples GTSH2-300 and GTSH2-700. The diffraction pattern of GTSH2-300 has broad peaks, indicating a disordered nature. The GTSH2-700 pattern has narrow peaks, indicating a more ordered crystal structure. (b) X-ray patterns for samples MTSH4-400 and MTSH4-700. The peaks present in the MTSH4-400 pattern that are not seen in the MTSH4-700 pattern are indicative of maghemite. The MTSH4-700 pattern has much narrower hematite peaks than the MTSH4-400 sample, indicating greater crystallinity. (c) X-ray patterns for natural samples DUR1, ODH3, and SWAN1. Sample DUR1 is almost pure well-crystalline hematite. Sample ODH3 is primarily well-crystalline hematite but contains impurities identified as phyllosilicates and sulfide minerals. Sample SWAN1 has abundant quartz because of the hematite coating's host rock. A small goethite peak is present, and some of the hematite peaks are broad, as was seen in synthetic sample GTSH2-300.

4.5.2. GTSH3 Series

[34] Emission spectra of the GTSH3 series are shown in Figure 10. The results of heating the GTS3 precursor are similar to the results obtained by heating the GTS2 precursor. As with the GTSH2 series, spectral variations occur with heating temperature (250° to 700°C). The GTS3 precursor and sample GTSH3-250 have similar spectra. Both have emissivity minima at 893 and 795 cm^{-1} that are not present in hematite spectra. Additional emissivity minima are present at 595, 471, 429, 432, 402, and 268 cm^{-1}, although the minimum at 595 cm^{-1} is very weak in the GTSH3-250 spectrum. There is no indication of hematite spectral features in the GTSH3-250 spectrum. Emissivity spectra indicate that the first sample completely transformed to hematite is GTSH3-300. The minima present at 893 and 795 cm^{-1} in the GTS3 and GTSH3-250 spectra are not present in the GTSH3-300 spectrum. A major absorption band appears at 541 cm^{-1} in the GTSH3-300 spectrum. Additionally, the broad bands at 471 and 402 cm^{-1} in the GTS3 and GTSH3-250 spectra are replaced by a single minimum at 444 cm^{-1} in the GTSH3-300 spectrum. The minimum at 268 cm^{-1} seen in the GTS3 and GTSH3-250 spectra is replaced by a 310 cm^{-1} minimum with a resultant shift of the emissivity maximum from 309 to 371 cm^{-1} in the GTSH3-300 spectrum. For samples GTSH3-500 and higher an absorption at 381 cm^{-1} appears and becomes more pronounced as the temperature of dehydroxylation increases. As seen in the GTSH2 series, an additional effect of the increasing heating temperature is the effective broadening of the absorption band at 541 cm^{-1}.

4.5.3. GTSH4 Series

[35] Emission spectra of the GTSH4 series are shown in Figure 11. The results of heating the GTS4 precursor are

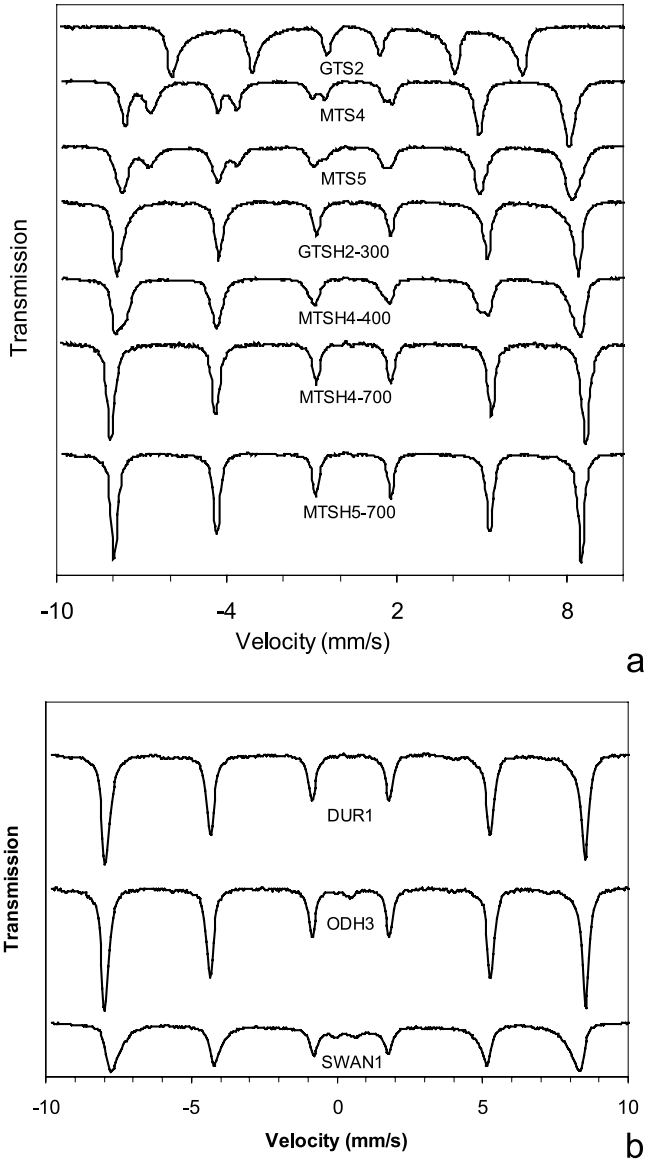

Figure 8. (a) Mössbauer spectra (293 K) of samples GTSH2-300, MTSH4-400, MTSH4-700, and MTSH5-700. All samples are characterized by the hematite sextet, except for MTSH4-400, which also shows a contribution from maghemite. For reference, spectra of goethite GTS2, magnetite MTS4, and hematite HMS3 [*Morris et al.*, 1985] are also shown. The vertical dashed lines are located at the positions of the outer lines of the hematite sextet. (b) Mössbauer spectra (293 K) for the three natural samples DUR1, ODH3, and SWAN1. Their spectra are dominated by the hematite sextet. The relaxed nature of the SWAN1 hematite sextet suggests poor crystallinity as also observed in XRD data.

Table 2. Summary of Mössbauer Spectral Parameters for Selected Synthetic Hematite Samples

Sample	IS, mm/s	QS, mm/s	Bhf, T	FWHM(1,6), mm/s
Synthetic Samples (This Study)				
GTSH2-300	0.37	−0.22	50.8	0.39
GTSH3-300	0.38	−0.19	50.7	0.39
GTSH4-300	0.38	−0.19	50.7	0.41
MTSH4-400[a]	0.37	−0.20	51.1	0.38
MTSH4-700	0.38	−0.19	51.7	0.31
MTSH5-700	0.37	−0.21	51.4	0.27
Synthetic Hematite Samples From Morris et al. [1985]				
HMS3	0.37	−0.22	51.1	0.25
HMS12	0.36	−0.22	51.3	0.25
HMS14	0.36	−0.22	51.2	0.25
Natural Samples (This Study)				
DUR1	0.36	−0.19	51.2	0.33
ODH3	0.36	−0.19	51.3	0.29
SWAN1	0.38	−0.21	51.2	0.55
Error	0.01	0.01	0.2	0.02

[a]Maghemite also present in this spectrum. Derived spectral parameters for modeled maghemite are IS = 0.28, QS = 0.09, Bh_f = 49.3, and FWHM = 0.49.

similar to the results obtained by heating the GTS2 and GTS3 precursors. The GTS4 precursor and sample GTSH4-250 have similar spectra, but there are more differences between these two samples than seen for the corresponding samples in the GTSH2 and GTSH3 series. Both the GTS4 and GTSH4-250 spectra have emissivity minima at 891 and 795 cm^{-1} that are not present in hematite spectra. Additional emissivity minima are present at 468, 406, and 271 cm^{-1}, although the absorption centered at 271 cm^{-1} is shallower in the GTSH4-250 spectrum than in the GTS4 spectrum. Despite the differences between the GTS4 and GTSH4-250 spectra, there is still no indication of hematite spectral features in the GTSH4-250 spectrum. Emissivity spectra show that the first sample completely transformed to hematite is GTSH4-300. The minima at 891 and 795 cm^{-1} in the GTS4 and GTSH4-250 spectra are not present in the GTSH4-300 spectrum. Additionally, a strong absorption appears at 541 cm^{-1} in the GTSH4-300 spectrum, and the broad absorptions at 468 and 406 cm^{-1} in the GTS4 and GTSH4-250 spectra are replaced by a single minimum at 445 cm^{-1}. As the dehydroxylation temperature increases further, the minimum at 271 cm^{-1} seen in the GTS4 and GTSH4-250 spectra is replaced by a 310 cm^{-1} minimum with a resultant shift of the emissivity maximum from 326 to 371 cm^{-1}. For samples GTSH4-400 and higher an

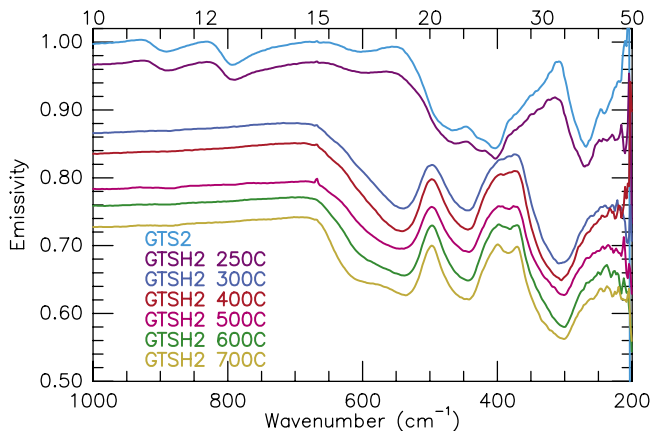

Figure 9. GTSH2 temperature-dependent spectral series. The GTS2 goethite powder and samples that resulted from heating are shown. Spectra are offset for clarity, and no contrast enhancement was performed on any of the spectra.

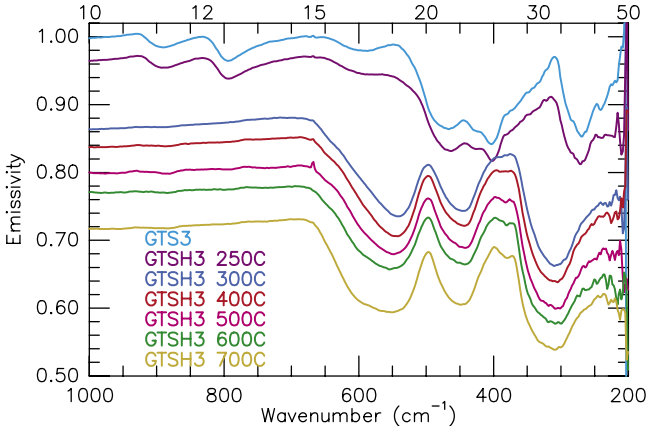

Figure 10. GTSH3 temperature-dependent spectral series. The GTS3 goethite powder and samples that resulted from heating are shown. Spectra are offset for clarity, and no contrast enhancement was performed on any of the spectra.

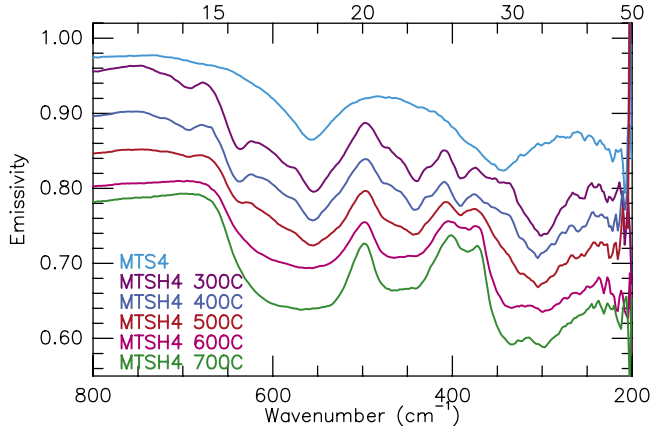

Figure 12. MTSH4 temperature-dependent spectral series. The MTS4 magnetite powder and samples that resulted from heating are shown. Spectra are offset for clarity, and no contrast enhancement was performed on any of the spectra.

absorption at 384 cm^{-1} appears and becomes more pronounced as the temperature of dehydroxylation increases. As seen in the GTSH2 and GTSH3 series, an additional effect of the increasing dehydroxylation temperature is the broadening of the absorption at 541 cm^{-1}. The effect is comparable to that seen in the other goethite precursor series.

4.5.4. MTSH4 Series

[36] Emission spectra of the magnetite precursor MTSH4 series are shown in Figure 12. The MTS4 precursor has an overall negative slope with decreasing wave numbers with emissivity minima centered at 558 and 343 cm^{-1}. Samples MTSH4-300 and MTSH4-400 have similar spectra. Modification of the magnetite is seen in the 300 degree and higher samples, as evidenced by the addition of several bands. Strong absorption bands resulting from hematite occur at 554, 442, and 301 cm^{-1}. The additional feature at 391 cm^{-1} is also consistent with hematite. Weak absorptions caused by the presence of maghemite (confirmed by XRD and Mössbauer) occur at 694 and 640 cm^{-1}. The strong absorptions correspond to hematite, but the additional minima indicate that at 300° and 400°C, the transition to hematite is still incomplete. Although a weak maghemite absorption is present at 694 cm^{-1}, the MTSH4-500 spectrum indicates that this sample is composed largely of hematite. Particularly, the strong absorptions at 442 and 301 cm^{-1} are better defined than in the spectra for the previously described samples in this series. The spectra of samples MTSH4-600 and MTSH4-700 are very similar, and they mark another major change in the series. The strong absorption bands are much broader and flat-bottomed. The emissivity minima shift to 561 and 457 cm^{-1}, and the 318 cm^{-1} feature is a doublet with emissivity minima occurring at 335 and 297 cm^{-1}. The doublet is likely the result of the expression of both E||**c** and E⊥**c** emission [*Onari et al.*, 1977]. The doublet nature is more pronounced in the MTSH4-700 spectrum than in the MTSH4-600 spectrum. Both sample spectra have absorptions at 388 cm^{-1} resulting from a (100) face emission contribution [*Lane et al.*, 2002].

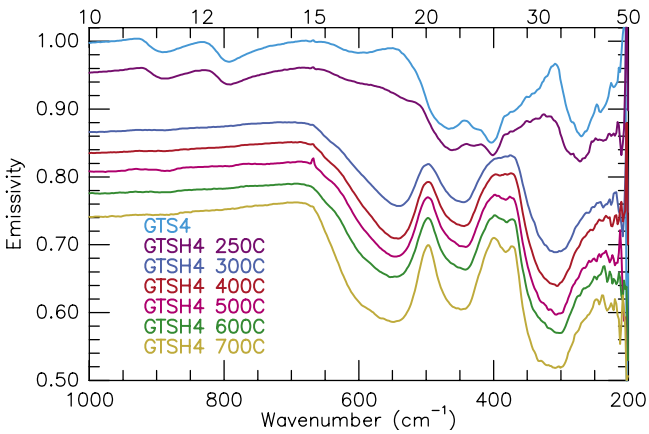

Figure 11. GTSH4 temperature-dependent spectral series. The GTS4 goethite powder and samples that resulted from heating are shown. Spectra are offset for clarity, and no contrast enhancement was performed on any of the spectra.

4.5.5. MTSH5 Series

[37] Emission spectra of the MTSH5 series are shown in Figure 13. The MTS5 precursor has an overall negative slope with major absorption bands at 554 and 350 cm^{-1} and a shallow local minimum at 441 cm^{-1}. Samples MTSH5-300 and MTSH5-400 have similar spectra. Numerous absorptions centered at 698, 640, 553, 479, 441, 421, 393, 366, 346, 303, and 258 cm^{-1} occur in both sample spectra, although the depths of some of these minima differ between the two spectra. The 553 cm^{-1} absorption results from the presence of magnetite. By analogy with sample MTSH4-400, the absorptions at 698 and 640 cm^{-1} are assigned to maghemite. The other absorptions are tentatively assigned to maghemite, as the conversion from magnetite to hematite is not complete at this stage of the heating process. The spectrum for the sample heated at 500°C (MTSH5-500) is the first in the series that resembles a hematite spectrum. Emissivity minima occur at 540, 451, and 305 cm^{-1}, and an additional local minimum is present at 383 cm^{-1}.

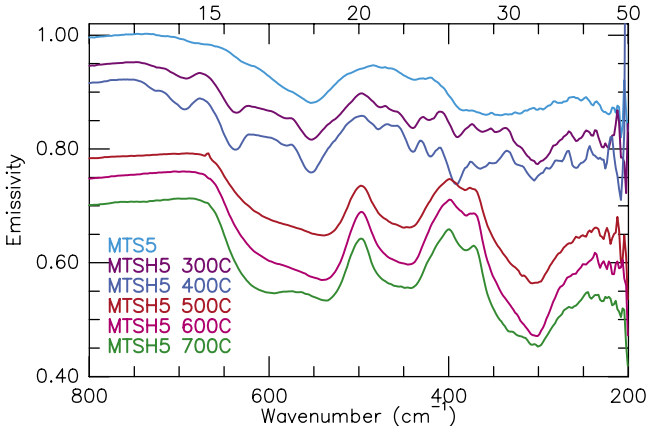

Figure 13. MTSH5 temperature-dependent spectral series. The MTS5 magnetite powder and samples that resulted from heating are shown. Spectra are offset for clarity, and no contrast enhancement was performed on any of the spectra.

The MTSH5-600 and MTSH5-700 spectra are similar. The strongest absorptions are in the same positions as in the MTSH5-500 spectrum, although the local absorption at 383 cm^{-1} becomes more pronounced as the heating temperature is increased. The MTSH5-700 spectrum has an additional minimum at 600 cm^{-1}.

4.5.6. Natural Hematite Samples

[38] Figure 14a shows emissivity spectra of the three natural hematite samples described in section 3.1.3. The Durango hematite sample (DUR1) spectrum has strong absorption bands at 552, 460, and 312 cm^{-1}, with a local emissivity minimum at 394 cm^{-1}. A striking feature of this spectrum is the depth of the 552 cm^{-1} absorption band. It has a much lower emissivity than the 460 cm^{-1} absorption, to a degree not seen in any of the synthetic hematite spectra.

[39] The Olympic Dam hematite (ODH3) has emissivity minima located at 540, 477, and 296 cm^{-1}, and a prominent 390 cm^{-1} feature is present. There are three oscillators in the 400–530 cm^{-1} region [*Onari et al.*, 1977], and the variation in their relative energies between the samples can explain the minimum being present at 460 cm^{-1} in the DUR1 sample and 477 cm^{-1} in the ODH3 sample. The variation in band intensity is also indicated by the thermal emission spectra of MTSH4-700 and MTSH5-700, which have emissivity minima near 469 and 443 cm^{-1}, respectively. It is also possible that impurities in the ODH3 sample are affecting the spectral shape.

[40] By contrast, the Swansea hematite (SWAN1) spectrum is more similar to spectra of hematite derived from the pseudomorphic low-temperature (300° to 400°C) thermal decomposition of goethite in terms of band shapes and positions. It has well-defined emissivity minima at 545, 444, and 308 cm^{-1} and only a barely discernable local emissivity minimum at 391 cm^{-1}.

[41] The natural hematite samples have very little structure in the silicate-dominated 8–12 μm region of the spectrum (Figure 14b), indicating that silicate impurities are not likely to be affecting the major hematite bands.

5. Discussion

5.1. Comparison of Martian and Synthetic Hematite Thermal Emission Spectra

5.1.1. Comparison to the Martian Hematite Spectrum

[42] The thermal emission spectra of the synthetic hematites were resampled to MGS-TES sample intervals to permit direct comparison with the Martian hematite spectrum (Figure 15). Spectra are shown between 250 and 550 cm^{-1} to show the spectral region where differences in shape and position of the 300, 450, and 540 cm^{-1} absorption bands occur. All goethite-derived hematite spectra provide better matches for the Martian hematite spectrum than the magnetite-derived hematite spectra. Like the Martian hematite spectrum, the low-temperature (300°–400°C) goethite-derived sample spectra lack a 390 cm^{-1} feature. This feature is present in the higher-temperature sample spectra, although it is less prominent than in the magnetite-derived sample spectra. The shapes and positions of the absorption bands of the goethite-derived sample spectra are also comparable to the Martian hematite spectrum, although

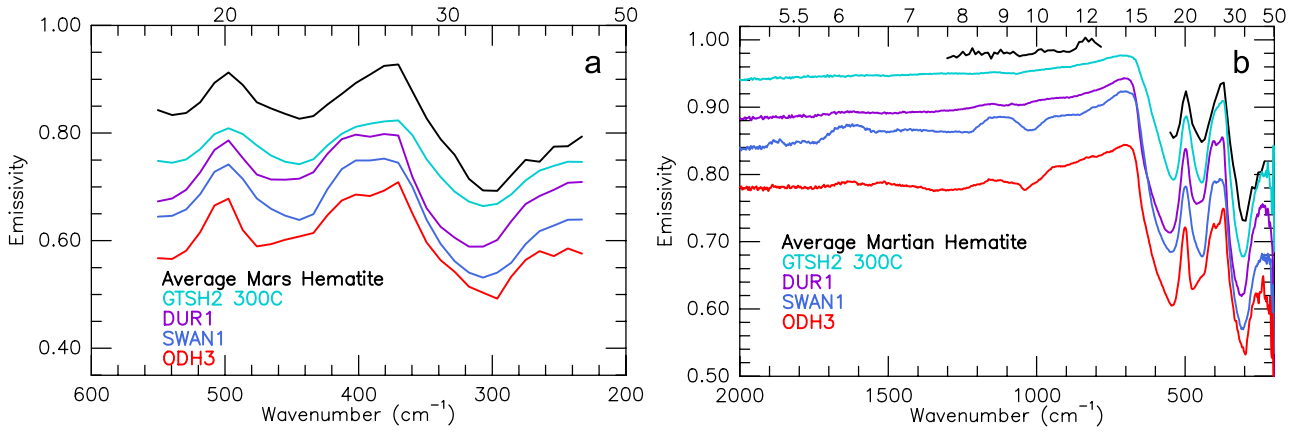

Figure 14. Spectra of Martian target-transformation derived hematite, laboratory sample GTSH2-300, and several natural hematite hand samples. (a) Laboratory and natural specimens are resampled to TES 10 cm^{-1} sampling and offset for clarity. (b) The natural sample spectra have very little structure in the 8–12 μm range, indicating that spectra are of nearly pure hematite.

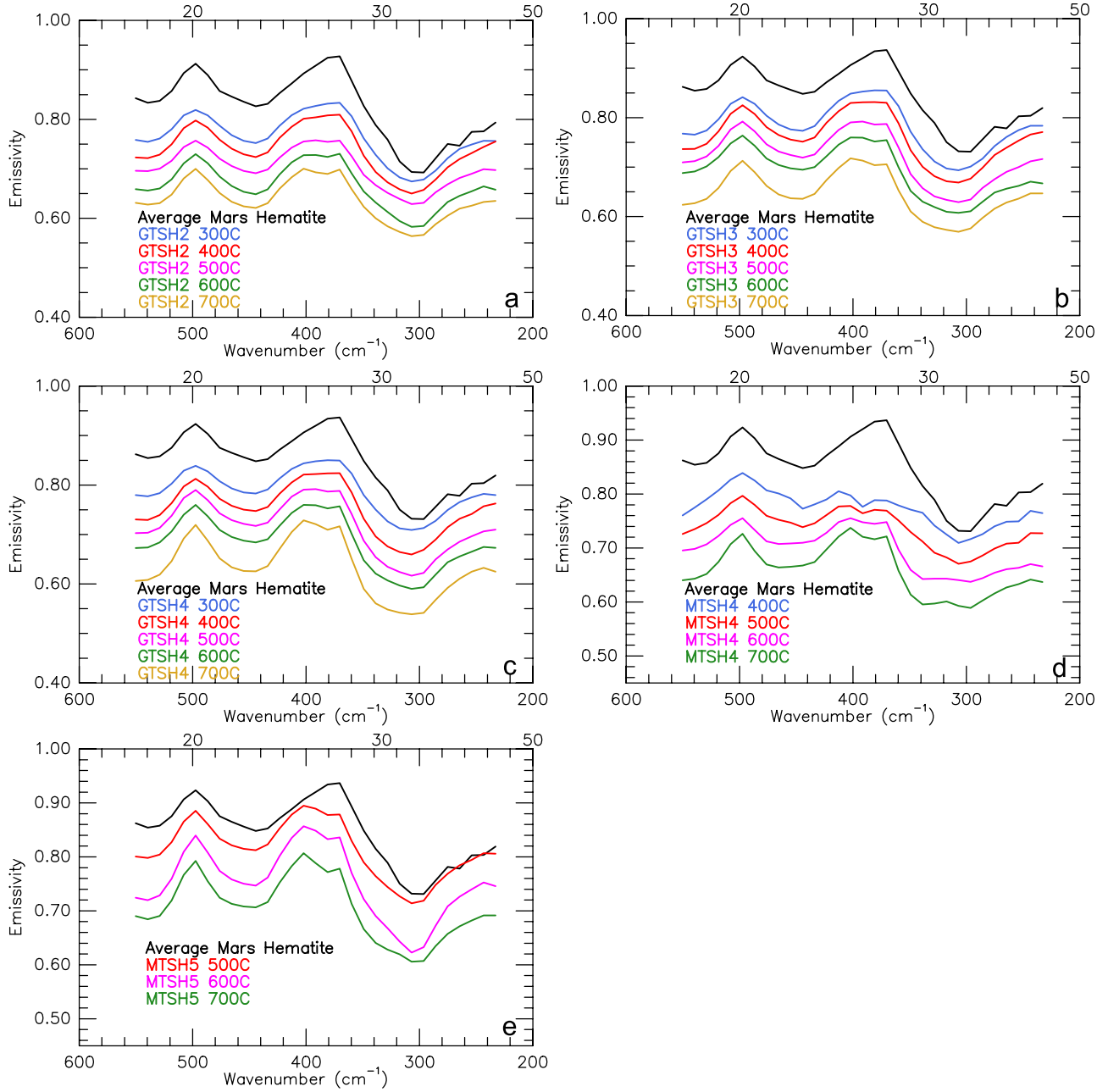

Figure 15. Spectra of the Martian target transformation derived hematite and laboratory hematites resampled to TES 10 cm^{-1} sampling. The Martian hematite spectrum is the top spectrum in each plot. Spectra are offset for clarity. (a) Comparison of the GTSH2, (b) GTSH3, (c) GTSH4, (d) MTSH4, and (e) MTSH5 hematite series with the Martian hematite spectrum. GTSH2-300 is the best overall fit for the Martian hematite.

the depth of the 300 cm^{-1} absorption tends to increase for the higher-temperature sample spectra, causing a decrease in the quality of the fit to the Martian hematite spectrum.

[43] Each magnetite-derived sample spectrum (Figures 15d and 15e) deviates significantly from the Martian hematite spectrum. Large differences are apparent in absorption band positions, shapes, and relative emissivities. Specifically, each magnetite-derived sample spectrum has a prominent 390 cm^{-1} feature, and in some cases the 300 cm^{-1} emissivity minimum is replaced by a doublet. In general, the MTSH5 series provides slightly better fits to the Martian spectrum than the MTSH4 series. This may be attributable to the fact that the MTS5 magnetite precursor was originally goethite. Additionally, crystal size differences between the MTS4 and MTS5 series and maghemite impurities in the MTS5 series may contribute to spectral differences between the two series. Each spectrum of the series has a prominent 390 cm^{-1} absorption, and especially at the higher temperatures, the band shapes are poor fits for the Martian hematite spectrum.

[44] Series GTSH2, and in particular sample GTSH2-300, provides the overall best fit for the Martian hematite

spectrum. Each of these samples lacks a 390 cm^{-1} feature, and the 540 cm^{-1} emissivity minimum in each spectrum is higher than that of the 450 cm^{-1} minimum. This is the case for the Martian hematite spectrum, but not for the other goethite-derived series or the magnetite derived series.

[45] The lack of a 390 cm^{-1} feature in the spectra of hematites derived topotaxially from goethite at the lowest decomposition temperatures indicates that the total-sample thermal emission is dominated by the {001} faces of hematite particles [*Onari et al.*, 1977; *Querry*, 1985; *Lane et al.*, 2002]. *Lane et al.* [2002] interpret this characteristic as evidence for microplaty hematite particles on Mars because this morphology has very large {001} faces. Our data show that an alternate interpretation is that the hematite particles are lath shaped, as occurs when hematite is derived from the dehydroxylation of goethite.

5.1.2. Measurement of Spectral Parameters

[46] Spectral parameters can be calculated for thermal emission spectra and used to quantitatively compare the Martian hematite spectrum to those obtained for terrestrial and analog hematite samples (Figure 16). The minimum emissivity value of the 540, 450, and 300 cm^{-1} absorption bands were measured. In order to directly compare the band shapes with the average Martian hematite spectrum, the widths of the 450 and 300 cm^{-1} absorption bands were measured at 0.85 and 0.71 emissivity (the FWHM values for the average Martian hematite spectrum), respectively, for each hematite spectrum. The baseline for the FWHM measurement was taken from the lower emissivity maximum corresponding to each emissivity minimum. To accurately compare the band widths of the spectra, the spectral contrast of each spectrum was set equal to the value for the Martian hematite spectrum. When the *Lane et al.* [2002] samples were set to the Martian spectral contrast, the minimum emissivities of the 300 cm^{-1} bands were above 0.71, so these samples are not plotted in the figures that contain that parameter. Band width errors are estimated to be about ± 1 cm^{-1}. Errors in band minimum position are estimated to be ± 0.1 cm^{-1}, and errors in minimum emissivity are estimated to be ± 0.001. In addition to the measured spectral parameters, the spectral root mean square error (RMS) between the Martian hematite spectrum, each sample spectrum (adjusted for contrast), and the five single-crystal (001) face hematite spectra from *Lane et al.* [2002] was calculated. The RMS values for each sample spectrum and the *Lane et al.* [2002] spectra are shown in Table 3. The lower-temperature goethite-derived samples tend to have the lowest RMS errors, while the single-crystal (001) face and higher-temperature goethite-derived and magnetite-derived samples have the highest RMS errors.

[47] The plots of spectral parameters (Figure 16) show clear trends in the properties of measured hematite spectra relative to the Martian hematite spectra based on their precursor mineralogy, temperature of formation, and, indirectly, crystallinity. In Figure 16a, Martian hematite clusters with the low-temperature (300°–400°C) goethite-derived laboratory hematite samples. The highest-temperature goethite-derived samples tend to plot farther away from the Martian spectrum than the lower-temperature goethite-derived samples. There is a large scatter in the magnetite-derived hematites, and the Olympic Dam natural hematite plots far away from the Martian hematite. The Swansea and Durango hematites fall in between the synthetic magnetite- and goethite-derived hematites. Figure 16b shows a much tighter cluster among all of the measured samples. The Martian hematite spectrum plots closest to a single magnetite-derived hematite. Otherwise, the goethite-derived hematites plot closest to the Martian spectrum. Again, there is a large scatter in the magnetite-derived samples. The Swansea hematite plots within the goethite-derived cluster, and the Durango hematite plots closest to a magnetite-derived hematite, although some high-temperature goethite-derived hematites are also nearby. Figure 16c shows the largest scatter among all of the samples. The Martian hematite has a higher $\varepsilon 450$ $cm^{-1}/\varepsilon 300$ cm^{-1} parameter than any measured sample. The *Lane et al.* [2002] **c** face samples have the lowest value of this parameter. There is an overall larger scatter in the positions of the goethite-derived hematites. The Swansea hematite is the natural sample that plots closest to the Martian hematite. Magnetite-derived hematites and the other natural hematite samples plot far away from the Martian hematite. Figure 16d again shows a tight cluster among the measured samples. The main difference between the *Lane et al.* [2002] **c** face samples and the other measured samples is the low $\varepsilon 450$ $cm^{-1}/\varepsilon 300$ cm^{-1} parameter, although these samples also have a higher 450 cm^{-1} band width parameter. In Figure 16e, Martian and SWAN1 hematites plot within the trend defined by the low- and high-temperature synthetic hematites derived from goethite. Magnetite-derived hematites and the other natural hematites plot far away from the Martian hematite. In Figure 16f the Martian and Swansea hematites plot at the low end of a trend defined by the low- and high-temperature goethite-derived hematites. The magnetite-derived hematites and the other natural samples plot at the high end of this trend because of a generally higher value of the $\varepsilon 450$ $cm^{-1}/\varepsilon 540$ cm^{-1} parameter. The *Lane et al.* [2002] **c** face samples plot away from the trend because of higher values for the 450 cm^{-1} band width parameter.

[48] A general observation from Figure 16 is that the spectral parameters for the spectra from the hematite derived pseudomorphically and topotaxially from goethite at low temperatures (<400°C) and SWAN1 are the most consistently similar to the spectral parameters for the Martian spectrum. For both the Martian surface and these terrestrial samples, the 390 cm^{-1} feature is not readily apparent in the emissivity spectra, and the band widths and relative band depths are comparable, although the Martian hematite spectrum does have a higher value of the $\varepsilon 450$ $cm^{-1}/\varepsilon 540$ cm^{-1} parameter than any measured sample. Higher-temperature (500°–700°C) goethite-derived sample spectra plot increasingly farther away from the Martian hematite spectrum in terms of the 450 cm^{-1} band width parameter. These sample spectra have distinct 390 cm^{-1} features which have a strong effect on this parameter.

[49] The spectra of the {001} faces of large single crystals of hematite [*Lane et al.*, 2002], with a few exceptions, plot far away from the Martian hematite. While these samples are analogs for the Martian hematite in that they have large {001} faces, and therefore no 390 cm^{-1} feature, their other spectral parameters are poorer matches for the Martian hematite. A characteristic of the goethite-derived hematite samples that are good matches to the Martian hematite spectrum is that they are all finely crystalline ($\sim 0.5-2$ μm). This may

be an important property with regards to the hematite spectral signature.

[50] In only rare cases do spectral parameters for hematites derived from a synthetic magnetite precursor plot close to the Martian hematite spectrum. This observation also holds for the natural sample that has a magnetite precursor (DUR1). The spectral parameters for sample ODH3 are anomalous, except in Figure 16d, where it plots in a cluster with the low-

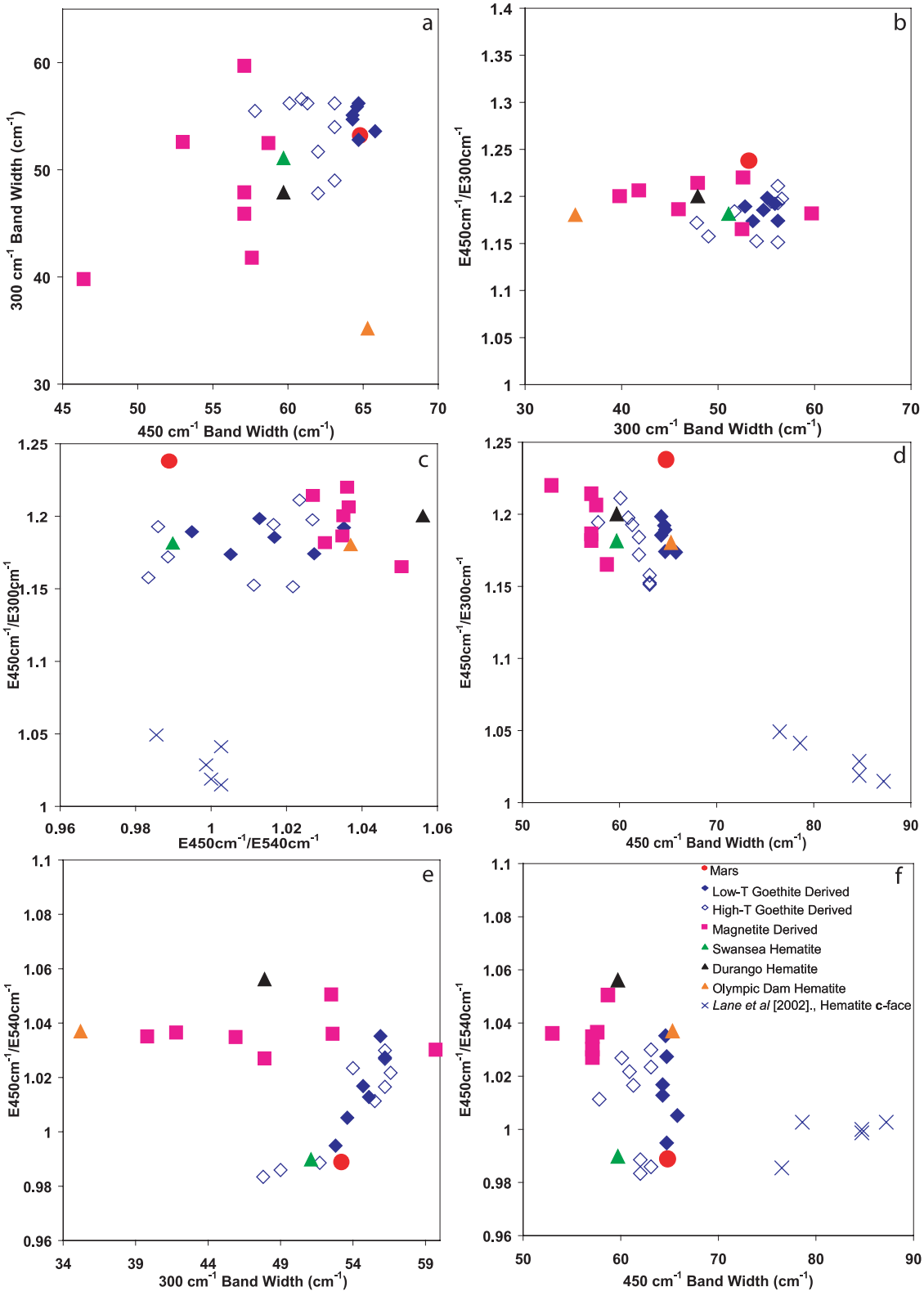

Figure 16

temperature goethite-derived hematites. Both ODH3 and SWAN1 were deposited by hydrothermal solutions, but the likely differences in the actual depositional environments, and the likelihood that SWAN1 had a goethite precursor, could be responsible for the differences in the spectral parameters of these two samples.

[51] In summary, by visual inspection, spectral RMS calculation, and quantitative spectral parameter analysis, the thermal emission spectra of natural hematite SWAN1 and synthetic hematites derived from goethite precursors by thermal dehydroxylation at $T \leq 300°C$ are the best match to corresponding Martian hematite spectra. Synthetic sample GTSH2-300 (goethite GTS2 precursor dehydroxylated at 300°C in a pseudomorphic and topotactic transformation) provides the best overall fit. Its cation ordering is poor (XRD and Mössbauer data), and the largest crystal surface is the (001) face.

5.2. Implications for Mars

[52] Several lines of evidence presented here indicate that the hematite-rich units on Mars were deposited initially in a relatively low temperature aqueous environment, possibly as goethite, and are in the form of fine-grained cements, coatings, and/or massive deposits. The emissivity spectra of lower-temperature (300°–400°C) goethite-derived hematite samples provide good fits to the Martian hematite spectrum. Infrared spectra of synthetic samples show that blade-shaped hematite samples derived from goethite lack a 390 cm^{-1} absorption feature, which is also missing from the Martian hematite spectrum. As the temperature of dehydroxylation of goethite to hematite increases, the 390 cm^{-1} feature appears and becomes more prominent. TEM photomicrographs show that the cause of this is growth of hematite crystals in random orientations. As sintering and recrystallization occur, the hematite {001} faces contribute less to the infrared spectrum, leading to the presence of the 390 cm^{-1} band. Both here and in *Lane et al.* [2002], the absence of the 390 cm^{-1} band is taken to imply that emission is dominated by {001} face emission from hematite.

[53] Of the natural hematite samples studied, the black hematite on sample SWAN1 provides the best thermal infrared spectral fit to the Martian hematite. The XRD pattern of this sample contains a small goethite peak and some broad hematite lines like those seen in synthetic hematite produced from goethite at temperatures below 600°C. The presence of both the goethite peak and the broad hematite lines indicates that the SWAN1 hematite sample is consistent with a goethite precursor mineralogy. Note that the Mössbauer and XRD spectra are applicable to the rind, because they were obtained on powders of bulk sample.

[54] In terms of band shapes, positions, and relative emissivities, infrared spectra of magnetite-derived hematite (both synthetic and natural) provide poor fits for the Martian hematite spectrum. Every magnetite-derived hematite sample spectrum has a strong 390 cm^{-1} absorption band not present in the Martian spectrum. TEM diffraction patterns indicate that emission from these samples is not dominated by the crystallographic {001} face. These data do not support previous suggestions [*Christensen et al.*, 2000; *Hynek et al.*, 2002; *Chapman and Tanaka*, 2002; *Arvidson et al.*, 2003] that the Martian crystalline hematite deposits are formed by water-free thermal oxidation of a magnetite-rich ash or lava.

[55] *Christensen et al.* [2000, 2001a] argued that hematite like that in Meridiani Planum was coarsely crystalline with discrete particles having diameters greater than ~10 μm. At smaller diameters the hematite becomes red in color [*Lane et al.*, 1999] and therefore not compatible with VNIR observations of the region. Because coarse-particulate hematite has a much greater spectral contrast than fine-particulate hematite in thermal emission spectra of pure

Table 3. Spectral RMS Error of Hematite Samples Deconvolved With the Martian Hematite Spectrum

Sample	RMS, %
This Study	
GTSH2-300	1.56
GTSH4-300	1.56
GTSH2-500	1.75
SWAN1	1.76
GTSH2-600	1.83
MTSH4-500	1.87
GTSH3-300	1.88
GTSH4-500	1.88
GTSH3-600	1.89
GTSH2-700	1.92
MTSH5-500	1.92
GTSH4-600	1.96
GTSH3-500	1.98
MTSH5-700	2.11
GTSH2-400	2.19
MTSH4-600	2.22
GTSH4-400	2.26
GTSH3-400	2.33
MTSH5-600	2.34
MTSH4-700	2.36
GTSH4-700	2.44
ODH3	2.44
DUR1	2.50
GTSH3-700	2.56
MTSH4-400	2.77
*Lane et al. [2002] Single-Crystal **c** Face Samples*	
HMRUS1	3.28
HMMG3	3.76
HMMG1	4.02
HMBB1	4.27
HMBME2	4.50

Figure 16. Hematite spectral parameters plotted against each other to quantitatively show how the laboratory and natural hematite samples compare to the Martian hematite spectrum. (a) 300 cm^{-1} FWHM band width plotted against the 450 cm^{-1} FWHM band width. (b) Ratio of the 450 cm^{-1} and 300 cm^{-1} band minimum emissivities plotted against the 300 cm^{-1} FWHM band width. (c) Ratio of the 450 cm^{-1} and 300 cm^{-1} band minimum emissivities plotted against the ratio of the 450 cm^{-1} and 540 cm^{-1} band minimum emissivities. (d) Ratio of the 450 cm^{-1} and 300 cm^{-1} band minimum emissivities plotted against the 450 cm^{-1} band width. (e) Ratio of the 450 cm^{-1} and 540 cm^{-1} band minimum emissivities plotted against the 300 cm^{-1} band width. (f) Ratio of the 450 cm^{-1} and 540 cm^{-1} band minimum emissivities plotted against the 450 cm^{-1} band width.

phases, deconvolution algorithms model the Martian hematite regions as roughly 10% coarse-particulate hematite or 60–70% fine-particulate, unpacked red hematite. Because having such a large amount of fine-particulate red hematite over areas as large as the deposits in Meridiani Planum and Aram Chaos was judged geologically unlikely and not compatible with the VNIR data [*Singer et al.*, 1979; *McCord et al.*, 1982; *Bell et al.*, 1990; *Mustard and Bell*, 1994; *Murchie et al.*, 2000], the coarse-particulate hematite was the preferred conclusion. The synthetic samples in this study are all red hematites, and even the "gray" natural samples exhibit a weak red spectral signature in the VNIR. For these samples to be consistent with the Martian hematite, either an additional stage of alteration (e.g., burial metamorphism [*Lane et al.*, 2002]) is required to make spectrally neutral hematite or the red VNIR spectral signature must be masked by other phases. Because the natural samples have a weak VNIR spectral signature, the latter alternative is more likely for the natural than the synthetic samples. Alternatively, precursor goethite on Mars could have been coarser than the material used in our study.

[56] *Lane et al.* [2002] further showed that the Martian hematite emissivity spectrum is consistent with emission dominated by the {001} faces of hematite because no 390 cm^{-1} absorption feature is present. All hematite samples used in their study that exhibited a Martian-like nature were very coarsely crystalline and had large {001} faces relative to their {100} faces because of microplaty-shaped particles. While these samples [*Lane et al.*, 2002, Figure 11] accurately reproduce the Martian hematite spectrum near 390 cm^{-1}, the shapes and positions of the major absorptions at 300 and 540 cm^{-1} are less similar than our low-temperature goethite-derived hematite samples to those seen in the Martian hematite spectra.

[57] Like the samples discussed by *Lane et al.* [2002], the low-temperature goethite-derived hematite samples presented here have large {001} faces. These samples also accurately reproduce the shapes and positions of major absorption bands at 300, 450, and 540 cm^{-1}. These samples, like those discussed by *Kirkland et al.* [2004], consist of particles that are significantly smaller than the 10 μm coarse hematite. The spectra of the "fine intimate" hematite coatings discussed by *Kirkland et al.* [2004], however, do not accurately reproduce the relative spectral depths between the major hematite spectral bands that are seen in the average Martian hematite spectrum. Specifically, the fact that the hematite coating 540 cm^{-1} band has a lower emissivity than the 450 cm^{-1} band is inconsistent with the average Martian hematite spectrum. Our work has shown this parameter to be important in identifying possible analogs to the Martian hematite.

[58] Higher-temperature synthetic hematite samples and natural coarsely particulate (>10 μm) samples presented here do not provide the same high-quality match to the Martian hematite emissivity spectrum over the range of features discussed. It is important to note, however, that the synthetic samples discussed here have crystal sizes (0.5–2 μm) that are still greater by an order of magnitude or more than nanophase hematite thought to be responsible for the color of the Martian dust [*Morris et al.*, 1989, 2000; *Morris and Lauer*, 1990; *Bell et al.*, 1990]. In summary, the data presented here suggest that the Martian hematite is crystalline, with crystal sizes on the order of ~0.5 to 2 μm that have large {001} faces. This is consistent with the aqueous deposition of goethite and later pseudomorphic thermal transformation at low temperature to hematite.

5.3. MER Instrumental Analysis

[59] The arrival of one of NASA's Mars Exploration Rovers (MER) and its suite of science instruments to the Meridiani Planum landing site will provide a unique opportunity to "ground truth" remote observations made by MGS-TES and the interpretations thereof with respect to the presence of hematite and its particle morphology and degree of crystallinity and purity. While the MGS-TES observations of the surface made from orbit must exclude the 540–772 cm^{-1} region because of the 667 cm^{-1} atmospheric CO_2 fundamental absorption, the MER Mini-TES [*Christensen et al.*, 2003] will be able to collect data in this range because it will be looking through a significantly smaller atmospheric column. The 540 cm^{-1} hematite absorption lies in this range, and as shown by our laboratory measurements, detailed characterization of this absorption band will provide additional information concerning the morphology, size, and distribution of Martian hematite and constrain its formation processes.

[60] The MER Mössbauer spectrometer [*Klingelhöfer et al.*, 2003] can detect minor iron oxide phases at much lower levels than is possible with Mini-TES. The presence of goethite, magnetite, or the other possible precursor minerals (e.g., ferrihydrite and maghemite) would also significantly constrain the interpretations of hematite formational mechanisms. Additionally, the measured Mössbauer parameters (IS, QS, and B_{hf}) and line shapes and intensities can be compared directly to the laboratory data, providing another test of the fidelity of the laboratory samples to the Martian hematite.

[61] Pancam will acquire multispectral data (~400–1000 nm) of the hematite deposit, and the Microscopic Imager (~30 μm/pixel) will provide direct photographic evidence of the particle size and morphology of the hematite [*Bell et al.*, 2003; *Herkenhoff et al.*, 2003]. The accurate determination of these parameters will have significant impact on the interpretation of the TES, Mini-TES, and laboratory emissivity spectra.

6. Conclusions

[62] Comparison of laboratory hematite spectra with the Martian hematite spectrum has resulted in the following conclusions:

[63] 1. Hematite spectral features vary significantly, and in a predictable way, with precursor mineralogy, temperature of formation, and crystal size (or degree of sintering). The presence and depth of a 390 cm^{-1} feature, as well as the width and relative depth of absorptions at 450 and 540 cm^{-1}, vary among the samples studied. Samples that have predominantly {001} face emission, which includes the lath-shaped hematite particles formed at low dehydroxylation temperatures from goethite (this study) and microplaty hematite particles formed by heating of iron oxides or hydroxides under high pressures [*Lane et al.*, 2002], show no 390 cm^{-1} absorption in thermal emission spectra.

[64] 2. All spectra of hematite derived from magnetite precursors have a significant 390 cm^{-1} feature because magnetite does not oxidize to hematite with large {001} faces. Similarly, samples of hematite formed from goethite at high temperatures have a significant 390 cm^{-1} absorption because sintering changed the shape of the hematite particles in a way that decreased the {001} surface area.

[65] 3. MGS-TES spectra of Martian surface regions with a hematite spectral signature do not show evidence for a 390 cm^{-1} band, implying that the hematite component of surface spectra is dominated by {001} emission [*Lane et al.*, 2002]. On the basis of comparison to the spectral features of laboratory samples, it is unlikely that the Martian hematite formations in Meridiani Planum, Aram Chaos, and Valles Marineris were formed as a result of thermal oxidation of magnetite, because of the presence of a 390 cm^{-1} feature and the poor match to the Martian hematite spectrum in other spectral parameters in samples of hematite derived from magnetite. This result does not support interpretations of the hematite unit as an oxidized magnetite-rich volcanic deposit.

[66] 4. The spectra of hematite derived from low-temperature (300°–400°C) alteration of goethite provide the best match to the mid-IR Martian hematite spectrum. These samples are poorly ordered, supporting a low-temperature origin for the Martian hematite. In addition, by analogy with terrestrial formation pathways for goethite, this result is consistent with an aqueous origin for the Martian hematite deposits by way of a goethite precursor. Martian goethite deposits could have been the result of aqueous weathering or direct aqueous precipitation. Low-grade burial metamorphism could have transformed the goethite to hematite [*Lane et al.*, 2002], but metamorphism is not necessary to produce microplaty hematite particles. As this work shows, topotactic alteration of lath-shaped goethite to hematite is sufficient. Although the lowest temperature in the laboratory at which goethite dehydroxylated to hematite was 300°C, the goethite dehydroxylation process occurs easily at much lower temperatures in nature, and goethite may be unstable relative to hematite under nearly all geologic conditions [*Berner*, 1969; *Langmuir*, 1971]. Although equilibrium conditions may not apply, goethite is thermodynamically unstable relative to hematite at current Martian surface conditions [e.g., *Fish*, 1966; *O'Connor*, 1968; *Gooding*, 1978].

[67] 5. Goethite initially precipitated as lath-shaped particles in a cement or a coating and subsequently dehydroxylated to hematite at low temperatures is an alternative explanation to burial metamorphism or precipitation of hematite under pressure for the spectral signature of hematite in Meridiani Planum, Aram Chaos, and Valles Marineris. Low temperatures (not greater than ~300°–400°C) are necessary to have a pseudomorphic transformation of goethite to hematite.

[68] 6. The Athena Science Package on the MER rovers will provide an excellent opportunity to test the hypotheses presented here. Comparison of hematite spectra from Mini-TES with the spectrum derived from MGS-TES will result in better interpretation of TES data. Pancam will assess the visual properties of the hematite deposit. Furthermore, the in situ science package consisting of the Mössbauer spectrometer, the Microscopic Imager, and the Alpha Proton X-Ray Spectrometer will greatly enhance our knowledge of the chemical makeup, particle morphology, and grain/crystal size of the hematite deposit.

[69] **Acknowledgments.** We would like to thank Melissa Lane and Janice Bishop for thoughtful reviews that significantly improved the manuscript. Deanne Rogers and Joshua Bandfield provided discussions and reviews of an early version of the manuscript. Joshua Bandfield also provided significant help with the target transformation and factor analysis used to derive the Martian hematite spectrum. Thanks to Kelly Bender, Kim Murray, Kim Homan, Noel Gorelick, Sadaat Anwar, and Greg Mehall at Arizona State University for their planning, acquisition, processing, and software support of the TES data. Additional thanks to Steven Reynolds for providing natural hematite samples used in this study and Kurt Leinenweber and the Arizona State University Multianvil Laboratory for use of their time and facilities. T.D.G. was supported by NASA GSRP grant NAG9-1131.

References

Arvidson, R. E., et al. (2003), Mantled and exhumed terrains in Terra Meridiani, Mars, *J. Geophys. Res.*, *108*(E10), 8073, doi:10.1029/2002JE001982.

Bandfield, J. L., P. R. Christensen, and M. D. Smith (2000), Spectral data set factor analysis and end-member recovery: Application to analysis of Martian atmospheric particulates, *J. Geophys. Res.*, *105*, 9573–9587.

Bandfield, J. L., K. S. Edgett, and P. R. Christensen (2002), Spectroscopic study of the Moses Lake dune field, Washington: Determination of compositional distributions and source lithologies, *J. Geophys. Res.*, *107*(E11), 5092, doi:10.1029/2000JE001469.

Barron, V., J. Torrent, J. P. Greenwood, and R. E. Blake (2004), Can the phosphate sorption and occlusion properties help to elucidate the genesis of specular hematite on the Mars surface?, *Lunar Planet. Sci.* [CD-ROM], *XXXV*, abstract 1853.

Bell, J. F., III, T. B. McCord, and P. D. Owensby (1990), Observational evidence of crystalline iron oxides on Mars, *J. Geophys. Res.*, *95*, 14,447–14,461.

Bell, J. F., III, et al. (2003), Mars Exploration Rover Athena Panoramic Camera (Pancam) investigation, *J. Geophys. Res.*, *108*(E12), 8063, doi:10.1029/2003JE002070.

Berner, R. A. (1969), Goethite stability and the origin of red beds, *Geochim. Cosmochim. Acta.*, *33*, 267–273.

Calvin, W. M., A. Fallacaro, and A. Baldridge (2003), Water and hematite: On the spectral properties and possible origins of Aram, Meridiani, and Candor, in *Sixth International Conference on Mars*, abstract 3075, Lunar and Planet. Inst., Houston, Tex.

Cambier, P. (1986), Infrared study of goethites of varying crystallinity and particle size: I. Interpretation of OH and lattice vibration frequencies, *Clay Miner.*, *21*, 191–200.

Catling, D. C., and J. M. Moore (2003), The nature of coarse-grained crystalline hematite and its implications for the early environment of Mars, *Icarus*, *165*, 277–300.

Chapman, M. G., and K. L. Tanaka (2002), Related magma-ice interactions: Possible origins of chasmata, chaos, and surface materials in Xanthe, Margaritifer, and Meridiani Terrae, Mars, *Icarus*, *155*, 324–339.

Christensen, P. R., and S. T. Harrison (1993), Thermal infrared emission spectroscopy of natural surfaces: Application to desert varnish coatings on rocks, *J. Geophys. Res.*, *98*, 19,819–19,834.

Christensen, P. R., et al. (2000), Detection of crystalline hematite mineralization on Mars by the Thermal Emission Spectrometer: Evidence for near-surface water, *J. Geophys. Res.*, *105*, 9623–9642.

Christensen, P. R., R. V. Morris, M. D. Lane, J. L. Bandfield, and M. C. Malin (2001a), Global mapping of Martian hematite deposits: Remnants of water-driven processes on early Mars, *J. Geophys. Res.*, *106*, 23,873–23,886.

Christensen, P. R., et al. (2001b), Mars Global Surveyor Thermal Emission Spectrometer experiment: Investigation description and surface science results, *J. Geophys. Res.*, *106*, 23,823–23,872.

Christensen, P. R., et al. (2003), The Miniature Thermal Emission Spectrometer for the Mars Exploration Rovers, *J. Geophys. Res.*, *108*(E12), 8064, doi:10.1029/2003JE002117.

Cornell, R. M., and U. Schwertmann (1996), *The Iron Oxides*, 573 pp., John Wiley, Hoboken, N.J.

Fallacaro, A., and W. M. Calvin (2003), Spectral and chemical characteristics of Lake Superior banded iron formation: Analog for Martian hematite outcrops, in *Sixth International Conference on Mars*, abstract 3067, Lunar and Planet. Inst., Houston, Tex.

Fish, F. F. (1966), The stability of goethite on Mars, *J. Geophys. Res.*, *71*, 3063–3068.

Gooding, J. L. (1978), Chemical weathering on Mars, *Icarus*, *33*, 483–513.
Greenwood, J. P., R. E. Blake, V. Barron, and J. Torrent (2004), P/Fe as an aquamarker for Mars, *Lunar Planet. Sci.* [CD-ROM], *XXXV*, abstract 1839.
Haynes, D. W., K. C. Cross, R. T. Bills, and M. H. Reed (1995), Olympic Dam ore genesis: A fluid mixing model, *Econ Geol.*, *90*, 281–307.
Herkenhoff, K. E., et al. (2003), Athena Microscopic Imager Investigation, *J. Geophys. Res.*, *108*(E12), 8065, doi:10.1029/2003JE002076.
Hynek, B. M., R. E. Arvidson, and R. J. Phillips (2002), Geologic setting and origin of Terra Meridiani hematite deposit on Mars, *J. Geophys. Res.*, *107*(E10), 5088, doi:10.1029/2002JE001891.
Johnson, J. R., P. G. Lucey, K. A. Horton, and E. M. Winter (1998), Infrared measurements of pristine and disturbed soils 1. Spectral contrast differences between field and laboratory data, *Remote Sens. Environ.*, *64*, 34–46.
Kirkland, L. E., K. C. Herr, and P. M. Adams (2004), A different perspective for the Mars rover "Opportunity" site: Fine-grained, consolidated hematite and hematite coatings, *Geophys. Res. Lett.*, *31*, L05704, doi:10.1029/2003GL019284.
Klingelhöfer, G., et al. (2003), Athena MIMOS II Mössbauer spectrometer investigation, *J. Geophys. Res.*, *108*(E12), 8067, doi:10.1029/2003JE002138.
Lane, M. D., R. V. Morris, and P. R. Christensen (1999), The spectral behavior of hematite at visible/near infrared and midinfrared wavelengths, in *Fifth International Conference on Mars*, *LPI Contrib. 972*, abstract 6085, Lunar and Planet. Sci., Houston, Tex.
Lane, M. D., R. V. Morris, S. A. Mertzman, and P. R. Christensen (2002), Evidence for platy hematite grains in Sinus Meridiani, Mars, *J. Geophys. Res.*, *107*(E12), 5126, doi:10.1029/2001JE001832.
Langmuir, D. (1971), Particle size effect on the reaction goethite = hematite + water, *Am. J. Sci.*, *271*, 147–156.
Lyons, J. I. (1988), Volcanogenic iron oxide deposits, Cerro de Mercado and vicinity, Durango, Mexico, *Econ. Geol.*, *83*, 1886–1906.
McCord, T. B., R. N. Clark, and R. B. Singer (1982), Mars: Near-infrared spectral reflectance of surface regions and compositional implications, *J. Geophys. Res.*, *87*, 3021–3032.
Morris, R. V., and H. V. Lauer Jr. (1981), Stability of goethite (α-FeOOH) and lepidocrocite (γ-FeOOH) to dehydration by UV radiation: Implications for their occurrence on the Martian surface, *J. Geophys. Res.*, *86*, 10,893–10,899.
Morris, R. V., and H. V. Lauer Jr. (1990), Matrix effects for reflectivity spectra of dispersed nanophase (superparamagnetic) hematite with application to Martian spectral data, *J. Geophys. Res.*, *95*, 5101–5109.
Morris, R. V., H. V. Lauer Jr., C. A. Lawson, E. K. Gibson Jr., G. A. Nace, and C. S. Stewart (1985), Spectral and other physiochemical properties of submicron powders of hematite (α-Fe_2O_3), maghemite (γ-Fe_2O_3), magnetite (Fe_3O_4), goethite (α-FeOOH), and Lepidocrocite (γ-FeOOH), *J. Geophys. Res.*, *90*, 3126–3144.
Morris, R. V., D. G. Argresti, H. V. Lauer Jr., J. A. Newcomb, T. D. Shelfer, and A. V. Murali (1989), Evidence for pigmentary hematite on Mars based on optical, magnetic, and Mössbauer studies of superparamagnetic (nanocrystalline) hematite, *J. Geophys. Res.*, *94*, 2760–2778.
Morris, R. V., et al. (2000), Mineralogy, composition, and alteration of Mars Pathfinder rocks and soils: Evidence from multispectral, elemental, and magnetic data on terrestrial analogue, SNC meteorite, and Pathfinder samples, *J. Geophys. Res.*, *105*, 1757–1817.
Murchie, S., L. Kirkland, S. Erard, J. Mustard, and M. Robinson (2000), Near-infrared spectral variations of Martian surface materials from ISM imaging spectrometer data, *Icarus*, *147*, 444–471.
Mustard, J. F., and J. F. Bell III (1994), New composite reflectance spectra of Mars from 0.4 to 3.14 μm, *Geophys. Res. Lett.*, *21*, 353–356.
O'Connor, J. T. (1968), Mineral stability at the Martian surface, *J. Geophys. Res.*, *73*, 5301–5311.
Onari, S., T. Arai, and K. Kudo (1977), Infrared lattice vibrations and dielectric dispersion in α-Fe_2O_3, *Phys. Rev. B*, *16*, 1717–1721.
Oreskes, N., and M. T. Einaudi (1992), Origin of hydrothermal fluids at Olympic Dam: Preliminary results from fluid inclusions and stable isotopes, *Econ. Geol.*, *87*, 64–90.
Querry, M. R. (1985), *Optical Constants*, contractor report, U.S. Army Chem. Res. and Dev. Eng. Cent., Aberdeen Proving Ground, Md.
Rendon, J. L., and C. J. Serna (1981), IR spectra of powder hematite: Effects of particle size and shape, *Clay Miner.*, *16*, 375–381.
Roddy, M. S., S. J. Reynolds, B. M. Smith, and J. Ruiz (1988), K-metasomatism and detachment-related mineralization, Harcuvar Mountains, Arizona; with Suppl. Data 88-22, *Geol. Soc. Am. Bull.*, *100*, 1627–1639.
Ruff, S. W., P. R. Christensen, P. W. Barbera, and D. L. Anderson (1997), Quantitative thermal emission spectroscopy of minerals: A laboratory technique for measurement and calibration, *J. Geophys. Res.*, *102*, 14,899–14,913.
Salisbury, J. W., and A. E. Wald (1992), The role of volume scattering in reducing spectral contrast of restrahlen bands in spectra of powdered minerals, *Lunar Planet. Sci.*, *XXIII*, 1205–1206.
Scott, I. R. (1987), The development of an ore reserve methodology for the Olympic Dam copper-uranium-gold deposit, paper presented at Resources Reserves Symposium, Sydney Branch, Australasian Inst. of Mining and Metall., Sydney, Nov.
Singer, R. B., T. B. McCord, R. N. Clark, J. B. Adams, and R. L. Huguenin (1979), Mars surface composition from reflectance spectroscopy: A summary, *J. Geophys. Res.*, *84*, 8415–8426.
Spencer, J. E., and J. W. Welty (1989), Geology of mineral deposits in the Buckskin and Rawhide Mountains, *Bull. 198*, pp. 223–254, Geol. Surv. Branch, Bur. of Geol. and Miner. Technol., State of Ariz., Tucson.
Stevens, J. G., A. Khasanov, J. W. Miller, H. Pollack, and Z. Li (1998), Documentation and evaluation of Mossbauer data for minerals, *Hyperfine Interact.*, *117*, 71–81.
Wilkins, J., Jr., R. E. Beane, and T. L. Heidrick (1986), Mineralization related to detachment faults: A model, *Ariz. Geol. Soc. Digest.*, *16*, 108–117.

P. R. Christensen, T. D. Glotch, and T. G. Sharp, Department of Geological Sciences, Arizona State University, Tempe, AZ 85287-6305, USA. (phil.christensen@asu.edu; tglotch@asu.edu; tom.sharp@asu.edu)
R. V. Morris, NASA Johnson Space Center, Code SR, Houston, TX 77058, USA. (richard.v.morris1@jsc.nasa.gov)